# Adsorption and Coadsorption of CO and NO on the Rh(100) Surface: A Theoretical Analysis

Dragan Lj. Vučković,[†] Susan A. Jansen, and Roald Hoffmann[*]

*Department of Chemistry and Materials Science Center, Cornell University, Ithaca, New York 14853-1301*

The adsorption of CO and NO and their coadsorption on the Rh(100) surface are discussed in terms of extended Hückel/tight binding calculations. Experimentally, it is not easy to resolve the linear and bent forms of NO, and for this reason our calculations serve not only as an examination of the proposed adsorption geometries but also as means to investigate the NO dissociation mechanism. This dissociation is believed to be the fundamental step in the CO/NO reaction. The adsorption site and geometry are discussed for several NO chemisorptions. In addition, a discussion of the CO/NO reaction for the proposed adsorption of NO is presented. From this analysis, it is clear that predissociation of NO into atomic components can lead to recombination producing the desired reaction products, $CO_2$ and $N_2$. Furthermore, the coadsorbate interactions can lead directly to the desired products.

The catalytic reduction of nitric oxide with carbon monoxide over transition-metal surfaces, forming $CO_2$ and $N_2$ as reaction products, is important in pollution abatement.[1] Among the transition metals, rhodium is the most effective catalyst for this purpose, and in the automotive exhaust environment it is the only catalyst which works efectively to reduce NO. Details of the catalytic mechanism are still somewhat unclear. In this work, we will study theoretically the coadsorption of CO and NO on the Rh(100) surface, as well as the behavior of each individual adsorbate.

Let us first review briefly some previous experimental and theoretical work in this area. The adsorption of CO on transition-metal surfaces has been studied extensively.[2-14] The experimental work has been accompanied by much theoretical consideration,[15-31] using a

whole variety of different methods, among which some have been reviewed recently.[32-35] On early transition metals, CO chemisorbs dissociatively, and on late transition metals molecularly.[2,16] On most rhodium surfaces, CO is adsorbed molecularly with the carbon end down. The adsorption geometrics and site preference for low-index Rh surfaces are well-known.[4-7] At lower coverages, the only CO state present is a molecular species in an on-top site, i.e., each CO being bound to a single Rh surface atom. With increasing CO coverage, a new compressed surface pattern is formed, with some CO starting to occupy two-fold bridging sites.[4-7,36] The simplest general picture of CO chemisorption postulates electron donation from the CO $5\sigma$ (HOMO) orbital into suitable transition-metal d orbitals and back-donation from the surface d orbitals into CO $2\pi$ (LUMO) orbitals. This is usually referred to as the Blyholder model.[37] There is some evidence that this simple picture may not be complete. Other CO orbit-

[†] Permanent address: The Boris Kidrič Institute of Nuclear Sciences, Vinča, Department of Chemistry 050, 11001 Belgrade, Yugoslavia.

(1) Kummer, J. T. *J. Phys. Chem.* **1986**, *90*, 4747.
(2) Broden, G.; Rhodin, T. N.; Bruckner, C.; Benbow, B.; Hurych, Z. *Surf. Sci.* **1976**, *59*, 593.
(3) Castner, D. G.; Sexton, B. A.; Somorjai, G. A. *Surf. Sci.* **1978**, *71*, 519.
(4) Dubois, L. H.; Somorjai, G. A. *Surf. Sci.* **1980**, *91*, 514.
(5) Baird, R. J.; Ku, R. C.; Wynblatt, P. *Surf. Sci.* **1980**, *97*, 346.
(6) Dubois, L. H.; Hansma, P. K.; Somorjai, G. A. *J. Catal.* **1980**, *65*, 318.
(7) DeLouise, L. A.; White, E. J.; Winograd, N. *Surf. Sci.* **1984**, *147*, 252.
(8) Plummer, E. W.; Chem, C. T.; Ford, W. K.; Eberhardt, W.; Messmer, R. P.; Freund, H.-J. *Surf. Sci.* **1985**, *158*, 58.
(9) Lesley, M. W.; Schmidt, L. D. *Surf. Sci.* **1985**, *155*, 215.
(10) Netzer, F. P.; Mack, J. U.; Bartel, E.; Matthew, J. A. D. *Surf. Sci.* **1985**, *160*, L509.
(11) Ishi, S.; Ohno, Y.; Viswanathan, B. *Surf. Sci.* **1985**, *161*, 349.
(12) Kuhlenbeck, H.; Saalfeld, H. B.; Neumann, M.; Freund, H.-J.; Plummer, E. W. *Appl. Phys. A* **1987**, *44*, 83.
(13) Rao, C. N. R.; Runga Rao, G.; Rajumon, M. K.; Prabhakaran, K. *Spectrochem. Acta A* **1987**, *43*, 1479.
(14) Lauth, G.; Solomun, T.; Hirschwald, W.; Christmann, K. *Surf. Sci.* **1989**, *210*, 201.
(15) Anderson, A. B.; Hoffmann, R. *J. Chem. Phys.* **1974**, *61*, 4545.
(16) Sung, S.-S.; Hoffmann, R. *J. Am. Chem. Soc.* **1985**, *107*, 578.
(17) Anderson, A. B.; Awad, Md. K. *J. Am. Chem. Soc.* **1985**, *107*, 7854.
(18) Cao, P.-L.; Wu, Y.; Chen, Y.-Q.; Zheng, D.-J. *Appl. Surf. Sci.* **1985**, *22/23*, 452.

(19) (a) Chen, Y.-Q.; Zheng, D.-J. *Wali Xuebao* **1985**, *34*, 1299 (Chinese). (b) Wa, Y.; Cao, P.-L.; Chen, Y.-Q.; Zheng, D.-J. *Wali Xuebao* **1985**, *34*, 1306 (Chinese).
(20) (a) Mehandru, S. P.; Anderson, A. B. *Surf. Sci.* **1986**, *169*, L281. (b) Mehandry, S. P.; Anderson, A. B. *Surf. Sci.* **1988**, *201*, 345.
(21) Andzelm, J.; Salahub, D. R. *Int. J. Quantum Chem.* **1986**, *XXIX*, 1091.
(22) Bagus, P. S.; Hermann, K.; Bauschlicher, C. W., Jr. *J. Chem. Phys.* **1984**, *81*, 1966.
(23) Müller, W.; Bagus, P. S. *J. Vac. Sci. Technol. A* **1987**, *5*, 1053.
(24) Hermann, K.; Bagus, P. S. *Appl. Phys. A* **1987**, *44*, 63.
(25) Hermann, K.; Hass, H. J. *Surf. Sci.* **1987**, *189/190*, 426.
(26) Wurth, W.; Schneider, C.; Treichler, R.; Umbach, E.; Menzel, D. *Phys. Rev. B* **1987**, *35*, 7741.
(27) Hermann, K.; Bagus, P. S.; Nelin, C. J. *Phys. Rev. B* **1987**, *35*, 9467.
(28) Kusuma, T. S.; Companion, A. L. *Surf. Sci.* **1988**, *195*, 59.
(29) (a) Gavezzotti, A.; Tantardini, G. F.; Meissner, H. *J. Phys. Chem.* **1988**, *92*, 872. (b) Ban, M. I.; Van Hove, M. A.; Somorjai, G. A. *Surf. Sci.* **1987**, *185*, 355.
(30) Wästberg, B.; Rosén, A. *Surf. Sci.* **1988**, *193*, L7.
(31) Broomfield, K.; Lambert, R. M. *Surf. Sci.* **1988**, *195*, L155.
(32) Simonetta, M. *Int. J. Quantum Chem.* **1986**, *XXIX*, 1555.
(33) Hoffmann, R. *Angew. Chem., Int. Ed. Engl.* **1987**, *26*, 846.
(34) Chulkov, E. V.; Silkin, V. M.; Lipnitskii, A. G.; Panin, V. E. *Electrochim. Acta* **1989**, *34*, 19.
(35) Sauer, J. *Chem. Rev.* **1989**, *89*, 199.
(36) Somorjai, G. A. *Chemistry in Two Dimensions: Surfaces*; Cornell University Press: Ithaca, London, 1981; p 280.
(37) Blyholder, G. *J. Phys. Chem.* **1964**, *68*, 2772. Doyen, G.; Ertl, G. *Surf. Sci.* **1974**, *43*, 197.

als may be important, especially $4\sigma$.[21,38] Also, the role of $2\pi$ orbitals and particularly the $5\sigma$ orbital has been questioned recently.[22–25,27,31] For a previous theoretical study of the CO chemisorption on transition-metal surfaces in this group, see ref 16.

Nitric oxide chemisorption on transition-metal surfaces has also been studied extensively.[2,5,6,9,39–44] It is much more complex and not as well understood as CO chemisorption. The NO ligand in both discrete complexes and on surfaces appears to have the freedom to bond linearly or bent. In nitrosyl transition-metal complexes, the extremes can be represented as M–(NO)$^+$ or M–(NO)$^-$, with the first leading to a linearly bonded and the latter to a bent NO configuration (NO axis being substantially tilted away from the surface normal).[44–48] In general, NO undergoes dissociative chemisorption more readily than CO. For NO on group VIII metals, there is evidence for low-temperature dissociative adsorption, as well as molecular adsorption in a variety of geometries, including a bent form, a bridged form, and a linear form.[49] However, unambiguous evidence for bent forms is difficult to obtain because of the complexity of the NO spectra.

The adsorption and decomposition of nitric oxide on rhodium have received some attention in the literature.[3,5,6,39,42,44,50,51] Both molecular chemisorption and dissociative chemisorption are found, with the latter leading eventually to $O_2$ and $N_2$ desorption. Just to illustrate the complexity of NO adsorption on Rh surfaces, it is worthwhile to mention that Dubois et al.[6] have reported at least five different NO species on Rh(111) using high-resolution EELS. For a detailed theoretical study of NO on Ni(111), see another contribution from this group.[52]

The CO/NO reaction on the transition metals has been investigated, for instance, on clean polycrystalline Pt,[53] Pt(111),[54] Pt(100),[9,55] and Ru(001).[56] In general, it is accepted that the NO dissociation is a prerequisite for the reaction to occur, at least for some surfaces. On surfaces such as Pt(111), in which NO is adsorbed only molecularly under ultra-high-vacuum conditions, no reaction with CO occurs.[53,54] The reaction was studied on the following rhodium surfaces: (110),[5] (331),[6] polycrystalline Rh,[57] (111),[58,59] (100),[59,60] (321), (331), and (533).[61] There have been numerous investigations of the CO/NO reaction over supported rhodium such as Rh/Al$_2$O$_3$[39,62] and Rh/SiO$_2$.[63] The basic question about the reaction mechanism is whether the major steps involve NO decomposition or if it is a true bimolecular reaction between adsorbed CO and NO. For the Rh(111) surface, it was recently shown[58e] that the mechanism goes exclusively through the NO decomposition step.

In an attempt to shed some more light on NO adsorption and its coadsorption and reaction with CO, we present here the theoretical investigation of the CO/NO system on a Rh(100) surface, using the extended Hückel/tight binding method.[64] This procedure has well-known deficiencies but in general describes simply the reactive trends responsible for surface chemistry.[33]

## Clean Rh(100)

The Rh(100) single-crystal surface is well defined and nonreconstructed,[3,50,60,65,66] giving a sharp (1×1) LEED pattern. For this reason, the model chosen for the calculation was a three-layer two-dimensional slab of the fcc rhodium metal structure[67] with a lattice constant of 3.8032 Å and nearest-neighbor separations of 2.6893 Å (1). Whether the use of the three-layer slab model to represent the surface in our calculation is appropriate has been discussed by this group in great detail earlier.[16,52,68,69]
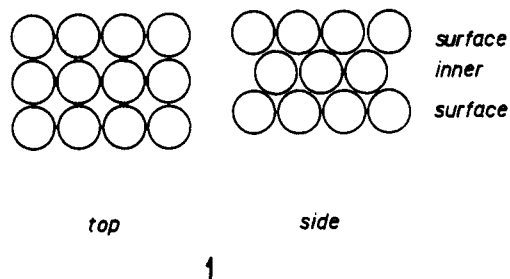
(38) (a) Miranda, R.; Wandelt, K.; Rieger, D.; Schnell, D. Surf. Sci. 1984, 139, 430. (b) Horn, K.; Bradshaw, A. M.; Hermann, K.; Batra, I. Solid State Commun. 1979, 31, 257. (c) Plummer, E. W.; Eberhardt, W. Adv. Chem. Phys. 1982, 49, 533. (d) Grevter, F.; Heskett, D.; Plummer, E. W.; Freund, H. J. Phys. Rev. B 1983, 27, 7117. (e) Loubriel, G.; Plummer, E. W. Chem. Phys. Lett. 1979, 64, 234. (f) Kasowski, R. V.; Rhodin, T.; Tsai, M.-H. Appl. Phys. 1986, A41, 61. Kasowski, R. V.; Tsai, M.-H.; Rhodin, T.; Chambliss, D. D. Phys. Rev. 1986, B34, 2688. Kasowski, R. V.; Tsai, M.-H.; Rhodin, T. N.; Chambliss, D. D. Solid State Commun. 1986, 59, 57. Kasowski, R. S.; Rhodin, T. N.; Tsai, M.-H., to be published.

(39) Arai, H.; Tominaga, H. J. Catal. 1976, 43, 131.

(40) Conrad, H.; Scala, R.; Stenzel, W.; Unwin, R. Surf. Sci. 1984, 145, 1.

(41) Umbach, E.; Kulkarni, S.; Feulner, P.; Menzel, D. Surf. Sci. 1979, 88, 65.

(42) Chin, A. A.; Bell, A. t. J. Phys. Chem. 1983, 87, 3700.

(43) DeLouise, L. A.; Winograd, N. Surf. Sci. 1985, 154, 79.

(44) DeLouise, L. A.; Winograd, N. Surf. Sci. 1985, 159, 199.

(45) Eisenberg, R.; Meyer, C. D. Acc. Chem. Res. 1975, 8, 26.

(46) Hoffmann, R.; Chen, M. M. L.; Elian, M.; Rossi, A. R.; Mingos, D. M. P. Inorg. Chem. 1974, 13, 2666.

(47) Enemark, J. H.; Feltham, R. D. Coord. Chem. Rev. 1974, 13, 339.

(48) Hoffmann, R.; Chen, M. M. L.; Thorn, D. L. Inorg. Chem. 1977, 16, 503.

(49) (a) Bonzel, H. P.; Pirug, G. Surf. Sci. 1977, 62, 45. (b) Pirug, G.; Bonzel, H. P.; Hopster, H.; Ibach, H. J. Chem. Phys. 1979, 71, 593. (c) Carley, A. F.; Rassias, S.; Roberts, M. W.; Wang, T.-H. Surf. Sci. 1979, 84, L227.

(50) (a) Ho, P.; White, J. M. Surf. Sci. 1984, 137, 103. (b) Ho, P.; White, J. M. Surf. Sci. 1984, 137, 117.

(51) Fisher, G. B. GM Research Report No. PC-289, 1985.

(52) Sung, S.-S.; Hoffmann, R.; Thiel, P. A. J. Phys. Chem. 1986, 90, 1380.

(53) Klein, R. L.; Schwartz, S.; Schmidt, L. D. J. Phys. Chem. 1985, 89, 4908.

(54) Gorte, R. J.; Schmidt, L. D. Surf. Sci. 1981, 111, 260.

(55) Schwartz, S. B.; Schmidt, L. D. Surf. Sci. 1988, 206, 169.

(56) Thiel, P. A.; Weinberg, W. H.; Yates, J. T. J. Chem. Phys. 1979, 71, 1643.

(57) Campbell, C. T.; White, J. M. Appl. Surf. Sci. 1978, 1, 347.

(58) (a) Root, T. W.; Schmidt, L. D.; Fisher, G. B. Surf. Sci. 1983, 134, 30. (b) Root, T. W.; Schmidt, L. D.; Fisher, G. B. Surf. Sci. 1985, 150, 173. (c) Fisher, G. B. GM Research Report No. PC-295, 1986. (d) Oh, S. H.; Fisher, G. B.; Carpenter, J. E.; Goodman, D. W. GM Research Publication GMR-5022, 1985. (e) Schwartz, S. C.; Fisher, G. B.; Schmidt, L. D. J. Phys. Chem. 1988, 92, 389.

(59) Peden, C. H. F.; Goodwin, D. W.; Blair, D. S.; Berlowitz, P. J.; Fisher, G. B.; Oh, S. H. J. Phys. Chem. 1988, 92, 1563.

(60) Hendershot, R. E.; Hansen, R. S. J. Catal. 1986, 98, 150.

(61) Hendrickx, H. A. C. M.; Winkelman, A. M. E.; Nieuwenhuys, B. E. Appl. Surf. Sci. 1987, 27, 458.

(62) Matyshak, V. A.; Slinako, M. M.; Gazarov, R. A.; Panchishnyi, V. I.; Kadushin, A. A.; Krylov, O. V., Kinetika y Kataliz 1986, XXVII, 167 (Russian).

(63) Rives-Arnau, V.; Munvera, G. Appl. Surf. Sci. 1980, 6, 122.

(64) (a) Hoffmann, R. J. Chem. Phys. 1963, 39, 1397. Hoffmann, R.; Lipscomb, W. M. Ibid. 1962, 36, 2176; 1962, 37, 2872. (b) Ammeter, J. H.; Bürgi, H.; Thibeault, J. C.; Hoffmann, R. J. Am. Chem. Soc. 1978, 100, 3686.

(65) Villarrubia, J. S.; Richter, L. J.; Gurney, B. A.; Ho, W. J. Vacuum Sci. Technol. A 1986, 4, 1487.

(66) Oed, W.; Dötsch, B.; Hammer, L.; Heinz, K.; Müller, K. Surf. Sci. 1988, 207, 55.

(67) Donohue, J. The Structure of the Elements; Kreiger, R. E., Publ. Comp., Inc.: Malabar, FL, 1982; p 215.

(68) Zonnevylle, M. C.; Hoffmann, R. Langmuir 1987, 3, 452.

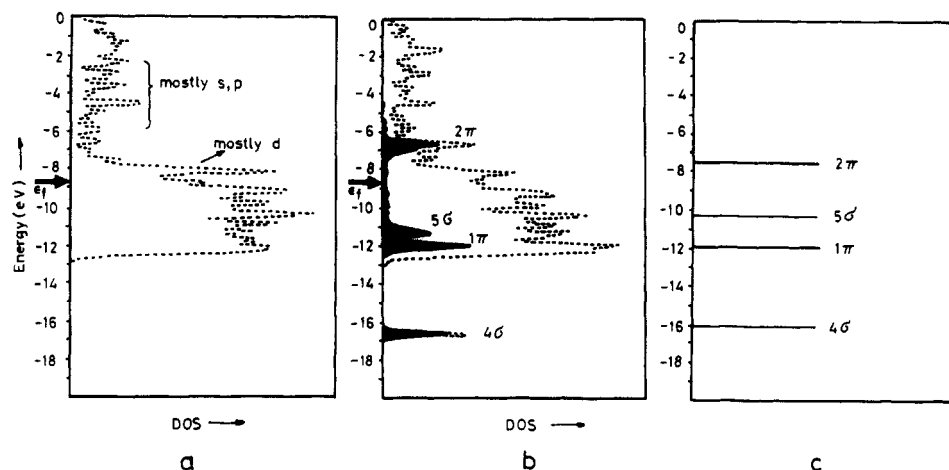(69) Saillard, J.-Y.; Hoffmann, R. J. Am. Chem. Soc. 1984, 107, 2006.

**Figure 1.** (a) Total DOS of the three-layer slab, with Fermi level ($\epsilon_f$) and s, p, and d bands indicated. (b) Total DOS of the c(2×2) CO–Rh(100) system (broken line) and projected DOS of adsorbed CO molecule (black areas), with the main contributions from the CO orbitals marked. (c) Energy levels of an isolated CO molecule.

The calculated density of states for a three-layer slab shows a d band between -7.0 and -13.0 eV and dispersed s and p bands starting from -12.0 to 20 eV. The Fermi level is at -8.55 eV (Figure 1a). Since the surface atoms have a lower coordination number than the bulk atoms, their states are less dispersed than the bulk states. If the Fermi level falls above the midpoint of the d block, as it does for rhodium, then the surface should have a negative charge with respect to the bulk. This behavior of the electron density at the surface as a function of electron count has been discussed earlier by the members of this group[69] and others.[70] In our case, the total charge on the surface rhodium atom is an exaggerated 9.32 electrons, and the bulk atoms have a total of 8.35 electrons. In reality, the metal surfaces are neutral. This disagreement may be a mere artifact of the MO concept used. It is worthwhile to note that some other cluster (pseudopotential[29a] or MO[29b]) calculations also lead to different charges on different atoms in the cluster. On the other hand, the effective charges themselves are not well-defined properties.

## CO on the Rh(100) Surface

CO readily chemisorbs on the Rh(100) surface with a sticking coefficient near unity. The chemisorption is molecular, and no evidence for dissociation was observed. On the Rh(100) surface, CO site preference is coverage and temperature dependent.[3,71] At lower exposures, a c(2×2) adsorption LEED pattern was observed and at higher exposures above 1 langmuir this structure is compressed into a hexagonal overlayer, which is a split (2×1) pattern. The saturation coverage is about $\theta = 0.82$. At lower temperatures (~100 K), some other complicated structures were observed[71] similar to the coincidence lattice pattern reported by Tucker,[72] with a rectangular unit cell which is 4 × 1 times the rhodium face-centered cell. This result was later questioned by Castner et al.[3] since it was unclear whether these studies were carried out on an initially clean surface. Kim et al.[71a] have found a similar compressed structure.

In general, we can say that at lower exposure a regular c(2×2) pattern (coverage of 0.5) is observed with the on-top adsorption geometry. Higher exposures lead to a compressed LEED structure with a saturation coverage near 0.8, involving a new adsorption state with a higher coordination number. This can be assigned to a twofold bridging state.[60] The difference of the heats of desorption between these two states was calculated by Hendershot and Hansen[60] to be 3.2 kcal/mol.

The molecular orbitals of an isolated CO are well-known.[73] The highest occupied molecular orbital (HOMO) is mainly the carbon lone pair 5σ (2a), and its energy is lower than the d states of most metals. In the generally
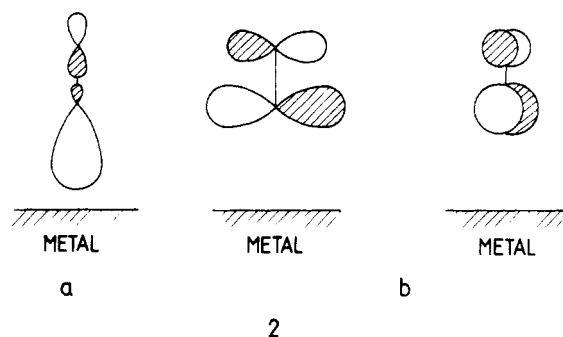


accepted picture of CO chemisorption, 5σ is stabilized through interaction with surface d states relative to other CO levels. The lowest unoccupied molecular orbital (LUMO) of the free CO molecule, the 2π, orbital consists of two antibonding combinations (2b) with larger coefficients on the carbon atom. As we have already mentioned, these two orbitals are mainly involved in the chemisorption mechanism (Blyholder model). Upon chemisorption, the 2π-derived orbitals are partially filled, and consequently, the CO bond is weakened. Aside from the frontier orbitals, other CO orbitals are usually not taken into account because they are too distant in energy from the active states of the surface. The general validity of the Blyholder model and the role of particular CO orbitals have been questioned recently,[12,14,22,23,31,74] though in some cases its validity was confirmed.[14,30]

(70) (a) Schustrovich, E. J. *J. Phys. Chem.* **1983**, *87*, 14. Beatzold, R. J. *J. Am. Chem. Soc.* **1983**, *105*, 4271. Shustrovich, E.; Beatzold, R.; Muetterties, E. L. *J. Phys. Chem.* **1983**, *87*, 1100. (b) Feibelman, P. J.; Hamann, D. R. *Solid State Commun.* **1979**, *31*, 413. Desjonqueres, M. C.; Spanjaard, D.; Lassailly, Y.; Guillot, C. *Ibid.* **1980**, *34*, 807.

(71) (a) Kim, Y.; Peebles, H. C.; White, J. M. *Surf. Sci.* **1982**, *114*, 363. (b) Peebles, D. E.; Peebles, H. C.; White, J. M. *Surf. Sci.* **1984**, *136*, 463.

(72) Tucker, C. W., Jr. *J. Appl. Phys.* **1966**, *37*, 3013.

(73) (a) Jorgensen, W. L.; Salem, L. *The Organic Chemist's Book of Orbitals*; Academic Press: New York, **1973**, pp 78, 80. (b) Huo, W. M. *J. Chem. Phys.* **1964**, *43*, 624. MacLean, A. D.; Yoshimine, M. *IBM J. Res. Dev. Suppl.* **1968**, *3*, 206.

(74) Gumhalter, B.; Wandelt, K. *Phys. Rev. Lett.* **1986**, *57*, 2318.

**Table I. Some Bonding Characteristics for c(2×2)CO on a Model Rh(100) Slab[a]**

| | | free CO | on-top | bridging |
|---|---|---|---|---|
| CO electron densities | $4\sigma$ | 2 | 1.78 | 1.72 |
| | $1\pi_x$ | 2 | 1.99 | 1.98 |
| | $1\pi_y$ | 2 | 1.99 | 1.95 |
| | $5\sigma$ | 2 | 1.67 | 1.69 |
| | $2\pi_x$ | 0 | 0.38 | 0.46 |
| | $2\pi_y$ | 0 | 0.38 | 0.76 |
| overlap populations | C–Rh | | 0.87 | 0.62 |
| | C–O | 1.44 | 1.23 | 1.09 |
| binding energy,[b] eV | | | 2.48 | 3.07 |

[a] $\theta = 0.5$. [b] Binding energy defined as $(E_{CO} + E_{Rh(100)}) - E_{CO+Rh(100)}$.

The band structure of an isoalted CO overlayer can be found in a previous contribution from our group on CO bonding to metal surfaces[16,33] as well as in the work of others.[12,38f] We will focus our attention only on the coverage and site dependence of CO chemisorbed on Rh(100). The results of our calculations are summarized in Table I. We have considered two adsorption geometries, on-top (3) and two-fold bridging (4), although it is known that an on-top adsorption is strongly preferred for lower coverages on the Rh(100) surface. The coverage depen-



3



4
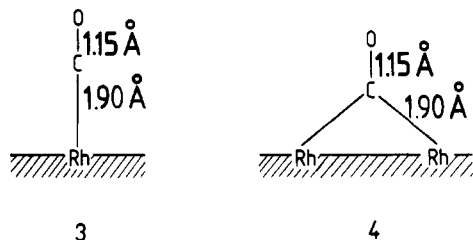
dence analysis was carried out for each adsorption geometry with three different coverages of the surfaces of 1, 1/2, and 1/4, which is represented by a top view in 5, 6, and 7, respectively. Table I, however, reports the results



5



6



7
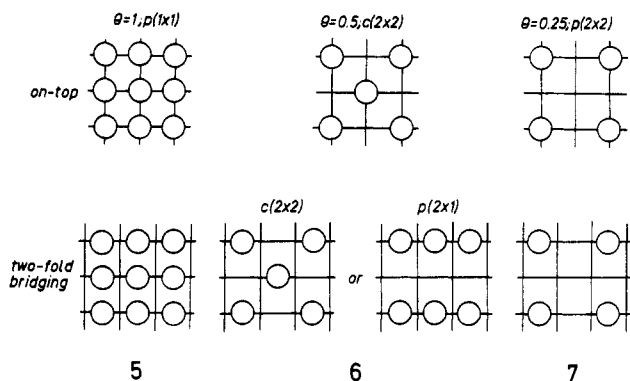
for one coverage, c(2×2) and $\theta$ = 0.5, because the results for other coverages are so similar. Note the forward donation in the depopulation of the $5\sigma$ (and $4\sigma$) and the back donation in the population of the $2\pi$. In the bridging mode, the degeneracy of the $\pi$ orbitals is, of course, lost; the greater back donation is to the $\pi$ orbital in the Rh–C–Rh plane, which is able to interact in $\sigma$ fashion with the Rh orbitals. With that greater back donation, there comes a greater weakening of the C–O bond. The binding energies cannot be relied on, because we assume and cannot optimize a Rh–C distance. Not much changes for other coverages, except that the binding energy, by its decrease, clearly shows that the CO molecules are uncomfortable compressed at $\theta$ = 1.0.

Let us look with a little more detail at the interactions in the on-top c(2×2)CO + Rh(100) system. At left in Figure 1 is the DOS (density of states) of a naked Rh(100) slab (Figure 1a), in the center (Figure 1b) the composite surface plus CO overlayer, and at right (Figure 1c) the energy levels of an isolated CO molecule. The density of states curve clearly shows that the major surface–adsorbate interaction involve $5\sigma$ and $2\pi$ CO orbitals, although the $4\sigma$ orbital is also shifted toward lower energies. The metal–CO $5\sigma$ interaction is mainly accomplished through electron donation to appropriate surface orbitals, i.e., $d_{z^2}$ which are pointed directly toward the $5\sigma$ and $4\sigma$ orbitals (8). The net result is depopulation of the $5\sigma$ and $4\sigma$ orbit-



8



9
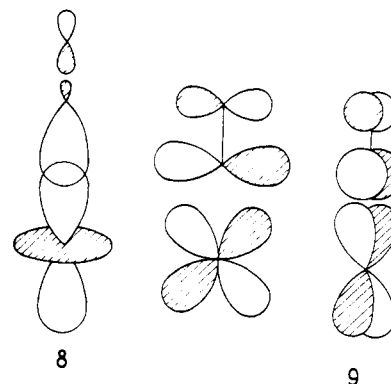
als from the two electrons each carry for a free CO molecule, to 1.67 and 1.78 electrons, respectively, in the composite system (Table I). As a result of this, the $5\sigma$ and $4\sigma$ orbitals are pushed down in energy (Figure 2a). The $d_{z^2}$ orbitals are pushed up, and consequently, a greater portion of the $d_{z^2}$ band is raised above the Fermi level. Another very strong metal–adsorbate interaction is through the CO $2\pi$ orbitals interaction with the surface $d_\pi$ orbitals ($d_{xz,yz}$), as represented schematically in 9. The initially empty $2\pi$ orbitals are now partly populated in the composite CO + Rh(100) system, with an electron density of 0.76 electron, while the corresponding surface $d_\pi$ states are depopulated.

Another way to follow the involvement of the various orbitals in bond formation is through the crystal orbital overlap population (COOP) analysis.[75] The COOP curve really represents an overlap population weighted density of states. It weights the states in each energy interval by their contribution to the overlap population. Such a COOP curve for C–O and C–Rh bonding in our c(2×2)CO + Rh(100) system is presented in Figure 3. The main CO orbital contributions are marked, and we can see that the $2\pi$ orbitals (i.e., their bonding combination with the $d_\pi$) are C–Rh bonding and C–O antibonding. The CO $1\pi$ orbitals are still the major bonding CO orbitals. The $5\sigma$ is both C–O and C–Rh bonding, but its absolute contribution to these bonds is small. On the other hand, the COOP curve shows that the $4\sigma$ makes a major contribution to C–Rh bonding.

What is the reason for large involvement of the $4\sigma$? One thinks $4\sigma$ is an oxygen-based lone-pair orbital, while $5\sigma$ is on carbon. Actually both are quite delocalized, and Table II shows their composition for free CO with our parameters. Unfortunately, the makeup of these orbitals is somewhat parameter dependent. One can see the delocalization in both. What really matters is the overlap these orbitals have with another group. With the parameters we have used, a probe H 1s orbital placed at
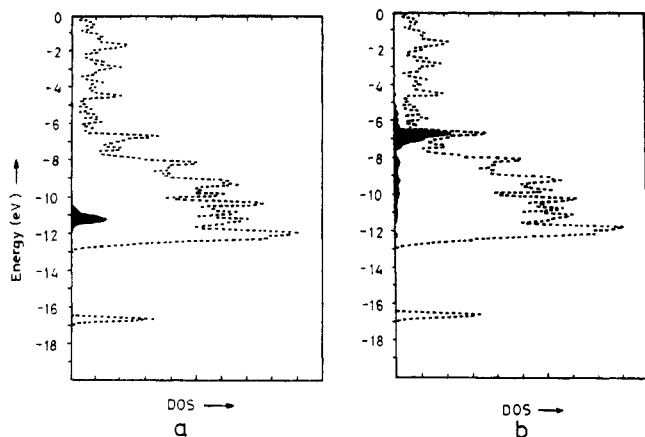
(75) Hughbanks, T.; Hoffmann, R. J. Am. Chem. Soc. 1983, 105, 1150.

**Figure 2.** Projected DOS (black areas) of $5\sigma$ (a) and $2\pi$ (b) CO orbitals in a c(2×2)CO-Rh(100) system. Broken lines represent the total DOS of the system. The peak between -16 and -17 eV is mainly the CO $4\sigma$.



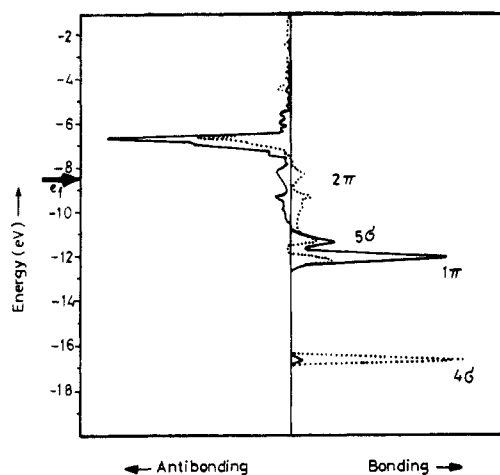**Figure 3.** Crystal orbital overlap population (COOP) curve for an on-top c(2×2)CO-Rh(100) system. Full line, carbon–oxygen bonding; dotted line, rhodium–carbon bonding.

**Table II. Wave Function Coefficients of Free CO $4\sigma$ and $5\sigma$ Molecular Orbitals with Our Parameters[a]**

|   |       | $4\sigma$ | $5\sigma$ |
|---|-------|-----------|-----------|
| C | s     | -0.7197   | 0.3308    |
|   | $p_x$ | 0.0000    | 0.0000    |
|   | $p_y$ | 0.0000    | 0.0000    |
|   | $p_z$ | 0.4051    | -0.4874   |
| O | s     | 0.2949    | 0.1147    |
|   | $p_x$ | 0.0000    | 0.0000    |
|   | $p_y$ | 0.0000    | 0.0000    |
|   | $p_z$ | 0.4362    | 0.7768    |

[a] See Appendix.

a distance 1.0–2.0 Å away from the carbon end of CO actually has a bigger overlap with $4\sigma$ than $5\sigma$. Still, its net interaction with $4\sigma$, though substantial, is less than with $5\sigma$ because $5\sigma$ is closer in energy to the hydrogen (or the frontier orbitals of a metal).

The CO $4\sigma$ orbital contribution to chemisorption in the present study might be overestimated by the use of charge-iterated parameters for carbon and oxygen atoms in CO overlayer on the rhodium surface (see Appendix). But even with the use of standard oxygen parameters in extended Hückel molecular calculations,[76] we had almost *the same effect as here. We note here also that others have suggested a significant role for the $4\sigma$ orbital.[38a,f]

---

(76) Hoffmann, R. *J. Chem. Phys.* **1963**, *39*, 1397.

## CO Bridging Site

We consider the bridging geometry in some detail, not because it is favored for CO on Rh(100), but because of the possibility that such a state may be involved in the coadsorption pattern with NO.

Our results for an adsorption geometry presented in **4** and for a c(2×2) LEED pattern (lower left part in **6**) are also presented in Table I. We have chosen the same C–Rh distance although it is known that bridge-bonded species should have somewhat longer distances.

The bonding here is a little bit more complicated. The CO $2\pi$ and $5\sigma$ orbitals still interact with the surface $d_{z^2}$ orbitals but less effectively. The corresponding bonding combinations are shown in **10** and **11**. In addition, both



10                                    11
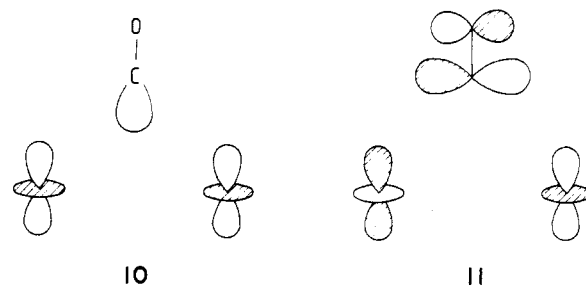
CO frontier orbitals can interact even more efficiently with the surface $d_{xz,yz}$ orbitals; the bonding combinations are shown in **12** and **13**. The $2\pi$ orbitals interact



12                                    13
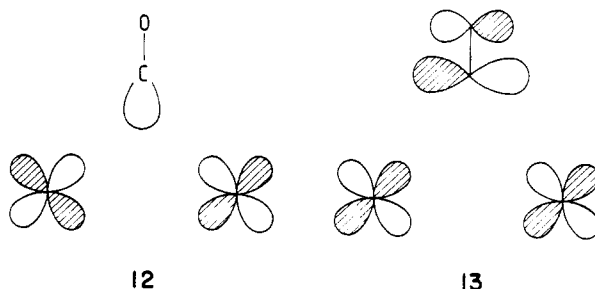
with surface antibonding $d_{xz,yz}$ orbitals (**13**), that is, with the upper part of the d band. Since the $2\pi$ energy falls just at that energy, the interaction is quite efficient. Thus, the filling of the CO $2\pi$ orbitals is higher in the bridging that in the on-top geometry (Table I). Consequently, the C–O overlap population is further reduced to 1.094 in a c(2×2) pattern, following the well-established trend that two-fold bridge-bonded species have a lower stretching frequency than terminally bonded ones.

It is very interesting to note that the $4\sigma$ orbitals are also active here. Even more so than in the on-top site, note in Table I the greater depopulation of $4\sigma$ for CO bridging.

## NO on the Rh(100) Surface

The chemisorption of nitric oxide on transition-metal surfaces has many similarities to that of CO but is more complex due to the additional geometrical possibilities (linear, bent) and the additional electron occupying the $2\pi$ orbital. For NO on group VIII transition metals, there is evidence for some low-temperature dissociative adsorption and a variety of molecular bonding geometries. These include a form with the NO axis tilted away from the surface normal (bent), a bridged form, and a linear one. For instance, the bent NO species were found on recon-

structed Pt(100)[77] and at lower coverages on Ni(111)[78-80] surfaces, with the latter being the subject of some controversy.[80] Both bent and linear forms of adsorbed NO were found at room temperature on polycrystalline Ni.[49c]

In 1979, Castner et al.[3] reported that NO chemisorption on the Rh(100) occurs with high initial sticking probability at 25 °C, forming a c(2×2) LEED structure. These workers stated that thermal NO desorption was complex. In the same year, Campbell and White[57] reported that a polycrystalline Rh sample at saturation had about 15% of dissociated NO. Ho and White[50] reported a low-temperature (~100 K) adsorption and decomposition study of NO on Rh(100). Adsorption was predominately molecular, with a small dissociative contribution at low coverages and a saturation coverage of 0.65 ML. The authors suggested that there are two major NO states involved in the chemisorption. The first corresponds to normal molecular adsorption, and the second has highly tilted NO molecules, such that both N and O atoms are bound to the surface with a weakened N--O bond. Upon heating, the latter decomposed before desorption. Later, Villarrubia et al.[65] resolved the vibrational modes of 920 and 1600 cm$^{-1}$ for two such different NO adsorption states at 90 K. The lower frequency state was attributed to a highly inclined or side-on (lying down) bonding mode of NO. A higher frequency state of about 1600 cm$^{-1}$ (more accurately at 1590 cm$^{-1}$ for low coverages, shifting to 1700 cm$^{-1}$ at higher coverages) was not unambiguously assignable to a specific adsorption site and geometry. Recently, the same group[81] reported a broad investigation on NO adsorption, decomposition, and desorption on the Rh(100) surface. They verified the existence of two major NO states, $\alpha_1$ (lying down) and $\alpha_2$ (vertically bonded one). Upon heating, 62% of NO decomposes, while the rest desorbs molecularly with $E_a = 28 \pm 3$ kcal/mol. The $\alpha_1$ NO decompose with $E_a = 10.5 \pm 0.7$ kcal/mol, while the decomposition of vertically bonded $\alpha_2$ NO is more complex, strongly coverage-dependent, and goes through a lying down $\alpha_1$ NO state as an intermediate. For a more detailed discussion of this subject, see, for example, ref 51, 52, 65, and 81.

It appears that for the chemisorption of NO on the Rh(100) surface we do not have enough experimental information to permit an unambiguous assignment of adsorption pattern and geometry. There is, however, some evidence that NO should adsorb vertically at two-fold bridging positions, since Villarrubia and Ho[81] in their model describing NO adsorption on Rh(100) placed vertically bonded $\alpha_2$ NO in the twofold bridging sites and the lying down $\alpha_1$ NO in the fourfold hollows. For some other Rh surfaces, such as Rh(111), G. B. Fisher and co-workers[51] reported that NO chemisorbs in twofold bridge sites at all coverages and that NO is partly dissociated at lower coverages (below 0.2 monolayer) with an activation energy for dissociation of 19 kcal/mol. At higher coverages, adsorption is molecular. Therefore, in order to examine adsorption and bonding of linearly bonded NO we performed an extended Hückel calculation for on-top and two-fold bridging geometries, for several coverages ranging from $\theta = 1$ to $\theta = 0.25$. The adsorption geometries used were the same as for CO adsorption coverages as in

**Table III. Some Bonding Characteristics for On-Top and Bridging c(2×2)NO + Rh(100) Systems$^a$**

| | | free NO | on-top | bridging |
|---|---|---|---|---|
| NO electron densities | $4\sigma$ | 2 | 1.85 | 1.81 |
| | $1\pi_x$ | 2 | 1.98 | 1.96 |
| | $1\pi_y$ | 2 | 1.98 | 1.89 |
| | $5\sigma$ | 2 | 1.71 | 1.73 |
| | $2\pi_x$ | 0.5 | 1.09 | 0.86 |
| | $2\pi_y$ | 0.5 | 1.09 | 1.27 |
| overlap populations | N–Rh | | 0.72 | 0.54 |
| | N–O | 1.16 | 0.89 | 0.91 |
| binding energy,$^b$ eV | | | 2.50 | 3.24 |

$^a$ $\theta = 0.5$. $^b$ Binding energy defined as $(E_{NO} + E_{Rh(100)}) - E_{NO+Rh(100)}$.

5, 6, and 7. Table III chooses again one typical coverage for a comparison.

NO chemisorption on Ni(111) has been examined earlier by this group.[52] The molecular orbitals of NO are very much like those of CO and therefore are the important interactions. Because of the extra electron and the low energy of the NO $2\pi$ orbitals, the total filling of the $2\pi$-derived orbitals of the composite system is much higher than for CO.

This system is less coverage-dependent than the corresponding CO system. This is indicated by calculations not reported here, in which one observes smaller changes in the N–O overlap populations when going from full to 1/4 coverage. Experimentally, the shift in stretching frequencies in low–high-coverage systems is very significant. On the other hand, it seems that our prediction as to which of these two different adsorption geometries is preferred, based on the "binding energies", is in agreement with the experiment, since for Rh(111)[51] and probably Rh(100)[81] the NO adsorption goes exclusively through a bridging geometry. For this geometry, our binding energy is considerably stronger.

It is interesting to note that the involvement of $4\sigma$ in adsorption, discussed for CO chemisorption, is also present here. The total effect is smaller than in CO, despite the smaller energy separation between the $4\sigma$ and $5\sigma$ levels. As for CO, this effect is stronger in the case of bridging geometry. The $4\sigma$ orbitals are more depopulated in this geometry (Table III).

## The Bending of NO

Here we want to investigate theoretically the proposed[50,81] multistep decomposition mechanism of vertically bonded NO that goes through the NO lying down geometry as an intermediate. A corresponding analysis of the NO + Ni(111) system[52] and of the bonding in discrete nitrosyls[46] was carried out by this group earlier. Thus we emphasize here only the most important features.

There are two likely ways of bending, from an on-top site and from the bridging position. For the sake of simplicity, we did all the calculations for the (2×2) geometry so that the coverages effects while bending are not included.

### Bending in the On-Top Site

Let us consider bending in an on-top site of NO adsorption, in a (2×2) geometry indicated in the upper drawing in 7. We will assume that the bending takes place in the $yz$ plane as shown in 14 in both perspective and top views. The bending or tilting angle $\phi$ is defined between
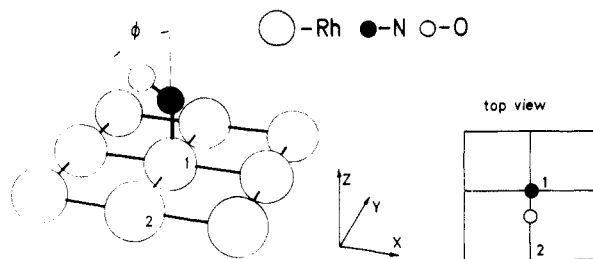
(77) Ibach, M.; Lehwald, S. *Surf. Sci.* **1978**, *76*, 1.

(78) Lehwald, S.; Yates, J. T., Jr.; Ibach, M. in *Proc. IVC-8, ICSS-4, ECOSS-3*, Cannes; Degres, D. A., Costa, M., Eds.; 1980; p 221.

(79) Reimer, W.; Fink, Th.; Küppers, J. *Surf. Sci.* **1988**, *193*, 259.

(80) Stainrück, H.-P.; Schneider, C.; Heimann, P. A.; Pache, T.; Umbach, E.; Menzel, D. *Surf. Sci.* **1989**, *208*, 136.

(81) Villarrubia, J. S.; Ho, W. *J. Chem. Phys.* **1987**, *87*, 750.

14

**Table IV. Bending of NO in the yz Plane[a]**

| | $\phi$ | 0° | 45° | 90° |
|---|---|---|---|---|
| NO electron densities | $4\sigma$ | 1.85 | 1.86 | 1.90 |
| | $1\pi_x$ | 1.98 | 1.98 | 1.97 |
| | $1\pi_{y(z)}$ | 1.98 | 1.98 | 1.90 |
| | $5\sigma$ | 1.71 | 1.77 | 1.83 |
| | $2\pi_x$ | 1.09 | 1.02 | 1.37 |
| | $2\pi_{y(z)}$ | 1.09 | 1.43 | 1.09 |
| overlap populations | N–O | 0.89 | 0.82 | 0.85 |
| | N–Rh(1) | 0.72 | 0.64 | 0.42 |
| | O–Rh(2) | | 0.00 | 0.12 |
| $d_{O-Rh(2)}$, Å | | | 4.07 | 3.30 | 2.44 |
| binding energy, eV | | 2.50 | 2.21 | 1.52 |

[a] Along the surface Rh–Rh bond in an on-top site (see 14).

the surface normal and the direction of the N–O bond. In 14, we give the coordinate system that will stay unchanged throughout this paper.

The results of our calculations are shown in Table IV as a function of bending angle $\phi$. As the bending angle increases from 0° to 45°, the N–O overlap population decreases, i.e., the NO bond is weakened. The N–Rh overlap population also decreases. The orientation of NO $5\sigma$ and $2\pi$ orbitals and the $d_{yz}$ and $d_{z^2}$ orbitals of the surface Rh are shown in 15 and 16. Upon bending, the ori-



15



16
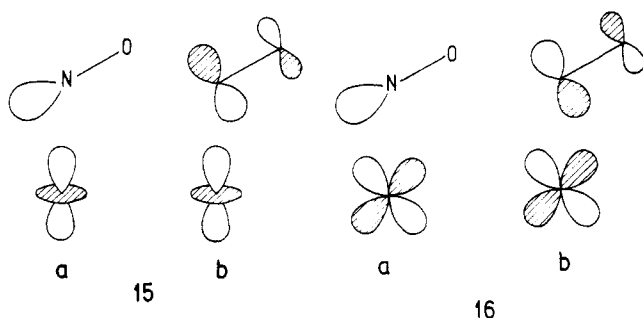
entation of the $5\sigma$ orbital enables it to interact with metal $yz$ orbitals, but this interaction is not strong enough to compensate for the loss in the $5\sigma$–$d_{z^2}$ interaction (8).

As the NO bends, $4\sigma$ and $5\sigma$ interact less with the metal. This is why their population moves toward 2.0. The $\pi_y$ and $\sigma$ orbitals mix and hybridize, so that $2\pi_y$ (really a mixture of $2\pi_y$ and $2\pi_z$) interacts with more orbitals of the metal, such as $d_{z^2}$, s, and $p_z$. Therefore, it gains more electron density than the $2\pi_x$ orbital. This increased occupation of antibonding levels is the main reason for weakening of the N–O bond in the bent geometry.

By further bending, $\phi = 90°$, we reach the situation shown in 17. The NO bond now lies parallel to the Rh(1)–Rh(2) surface bond, with the N atom being exactly on top of the Rh(1) atom. This geometry is particularly
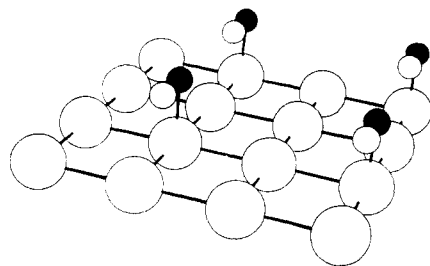


17

important since some similar states have been detected experimentally. This will be discussed in more detail

below, in a section analyzing possible geometries of NO parallel to the surface. Upon this further bending, the N–O overlap population increases somewhat and the N–Rh overlap population decreases further. On the other hand, the O–Rh(2) overlap population grows to the substantial positive value of 0.12 with the relevant atoms being 2.44 Å apart. Now we have a very interesting bonding pattern in which the $2\pi_z$ orbital interacts with the surface in the way the $5\sigma$ orbital did in the linear geometry, and the $5\sigma$ takes over the interaction with the Rh(1) $d_{yz}$ orbitals. The total NO–surface interaction is weaker, and the binding energy is reduced to only 1.52 (Table IV). We also studied further bending of NO up to 110°. The results are not reported in the table, but they continue the trend of N–O and N–Rh overlap populations decreasing further. It appears that this bending is not a good candidate for a dissociation mechanism pathway since the changes in the N–O overlap population do not show the required significant NO bond weakening.

Another possibility for bending in an on-top position is shown in 18. Now the bending is toward a fourfold



*top view*
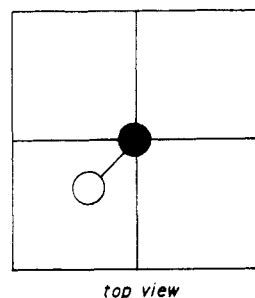
18

hollow, i.e., in the diagonal of the $xz$ and $yz$ planes. One is led to consider this variant as a precursor to N–O dissociation, because it is known that atomic species tend to occupy high-symmetry positions such as the fourfold hollow site.[82]

What happens in the calculations is that the binding energy decreases steadily and the NO overlap population behaves just as it did for bending "along a bond". So this bending toward a hollow does not look like a good prospect for the dissociative reaction pathway either.
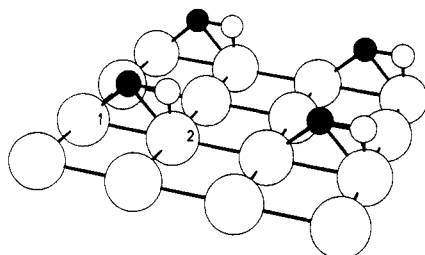
**Bending in a Bridging Position**

The two bending modes we single out for study are in the $yz$ plane (toward a hollow, 19) and in the $xz$ plane (toward a bond, 20). The first process, bending toward

(82) Fisher, G. B.; Schmieg, S. J. *J. Vacuum Sci. Technol. A* **1983**, *1*, 1064.

a hollow, does not seem to lead to anything new—once again the NO bond strengthens on 90° bending.
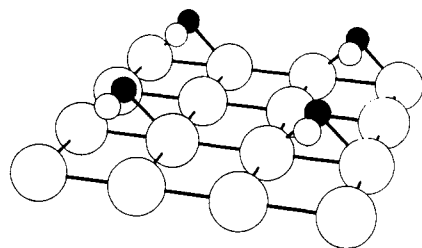


19



20

The second bending mode, **20**, is more interesting; the computational results for two bending angles are summarized in Table V. There are two entries for the N-Rh overlap populations since the bending is not symmetrical with respect to the Rh(1) and Rh(2) surface atoms. As NO bends, the orientation of the $\sigma$ and $\pi$ orbitals changes. Among these, the $2\pi_y$ orbital stays essentially the same, but there is a certain drop in the $2\pi_x$ (i.e., $2\pi_{x,z}$ for $\phi = 45°$) electron density. As a result, the N-O overlap population becomes larger. The bending of NO in the $x$ direction reduces the possibility of N-Rh(2) interaction since $5\sigma$ is moved away and directed more toward Rh(1). The corresponding overlap population is significantly reduced. The N-Rh(1) overlap population is somewhat increased. The overlap population between oxygen and the Rh(2) atom is still negative, so we still have an antibonding interaction here.

With further bending of NO to 90°, the situation changes a lot. The $4\sigma$-$5\sigma$ interactions with the surface Rh(1) and Rh(2) orbitals are increased and both of these orbitals are depopulated. There is a certain increase in $1\pi$ orbital interactions. The $2\pi_y$ orbitals are still almost unchanged, but the $2\pi_x$ (the $2\pi_z$ now) occupancy is getting larger. The $2\pi_z$ interacts in the way the $5\sigma$ interacted in the linear case and is filled as well. The net result of all of this is a significant weakening of the NO bond (note the decrease in the NO overlap population). The N-Rh(1) overlap population decreases. There is a very weak antibonding N-Rh(2) interaction, but a large increase in the O-Rh(2) overlap population, occurring mainly through the $4\sigma$ and surface $d_{zz}$ interactions. It must be said that the O-Rh(2) distance is much too short at 90°, so that bonding is overestimated. The binding energy increases at 90° in mode **20**, and finally we have found a way to weaken the NO bond. Perhaps this is the way the NO dissociates. But first let us examine a set of alternative geometries.

## Lying Down NO

In the preceding discussion, we have mentioned a few different geometries with the NO lying down, i.e., parallel to the surface. Such NO species, stable at lower tem-

peratures and coverages, have been observed experimentally on this surface. First, Ho and White[50] proposed an NO adsorption state with a weak NO bond and with both N and O interacting with the surface atoms for several desorption peaks observed in the thermal desorption of NO from Rh(100). Villarrubia et al.[65,81] recently reported a stable low-frequency NO species adsorbed on Rh(100), assigned it to either a highly inclined structure or one lying parallel to the surface, and proposed a model where lying down NO groups are occupying fourfold hollow positions. Similar $N_2$ adsorbed species have been observed on Fe(111).[83] Side-on-bonded CO molecules have also been reported on the Cr(110)[84] and Fe(100)[85] surfaces. A similar bonding mode of CN⁻ has also been reported.[86] Such experimental findings have been theoretically considered in the case of CO on the Cr(110) and different Fe surfaces by Mehandry and Anderson[20] and in the case of NO on various platinum surfaces by the Masel group.[87] The first group used an atom superposition and electron delocalization MO theory, with the surface represented by a two-layer-thick cluster of 21–33 chromium atoms.
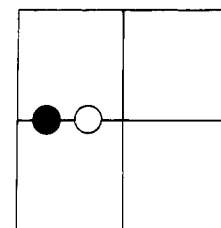
If we begin to study the bonding possibilities for NO lying down on a surface, we are led naturally to consider a set of geometries, **21–28**. **21**, **22**, and **24** have been dis-
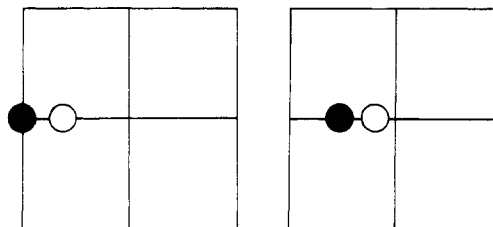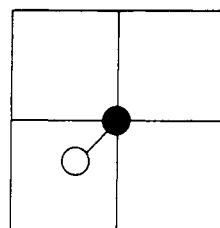


21
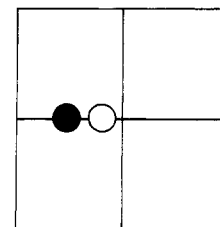


22



23



24
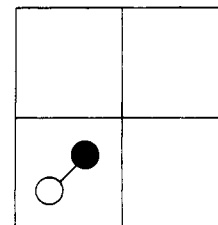


25

(83) (a) Grunze, M.; Golze, M.; Hirshwald, W.; Freund, H.-J.; Pulm, H.; Weip, U.; Tsai, M. C.; Ertl, G.; Kuppers, J. *Phys. Rev. Lett.* **1984**, *53*, 850. (b) Freund, H.-J.; Bartos, B.; Messmer, R. P.; Grunze, M.; Kuhlenbeck, H.; Neumann, M. *Surf. Sci.* **1987**, *185*, 187.

(84) (a) Shinn, N. D.; Madey, T. E. *Phys. Rev. Lett.* **1984**, *53*, 2481. (b) Shinn, N. D.; Madey, T. E. *J. Vac. Sci. Technol. A* **1985**, *3*, 1673. (c) Shinn, N. D.; Madey, T. E. *Phys. Rev. B* **1986**, *33*, 1464.

(85) Cameron, S. D.; Dwyer, D. J. *Langmuir* **1988**, *4*, 282.

(86) (a) Kordesch, M. E.; Steuzel, W.; Conrad, H. *Spectrosc. Relat. Phenom.* **1986**, *38*, 89. (b) Somers, J.; Kordesch, M. E.; Lindner, Th.; Conrad, H.; Bradshaw, A. M.; Williams, G. P. *Surf. Sci.* **1987**, *188*, L693.

(87) Banholzer, W. F.; Park, Y. O.; Mak, K. M.; Masel, R. I. *Surf. Sci.* **1983**, *128*, 176.

**Table V. Bending of NO in the *xz* Plane While Bridging (20)**

| | $\phi$ | 0° | 45° | 90° |
|---|---|---|---|---|
| NO electron densities | $4\sigma$ | 1.81 | 1.83 | 1.73 |
| | $1\pi_{x(z)}$ | 1.89 | 1.87 | 1.88 |
| | $1\pi_y$ | 1.96 | 1.95 | 1.81 |
| | $5\sigma$ | 1.73 | 1.75 | 1.64 |
| | $2\pi_{x(z)}$ | 1.28 | 0.95 | 1.27 |
| | $2\pi_y$ | 0.87 | 0.88 | 0.94 |
| overlap populations | N–O | 0.91 | 1.01 | 0.89 |
| | N–Rh(1) | 0.54 | 0.56 | 0.49 |
| | N–Rh(2) | 0.54 | 0.32 | -0.05 |
| | O–Rh(2) | | -0.03 | 0.71 |
| $d_{O-Rh(2)}$, Å | | | 2.83 | 2.22 | 1.37 |
| binding energy, eV | | 3.21 | 2.67 | 3.05 |

**Table VI. Various Possibilities of NO Lying Parallel to the Rh(100) Surface**

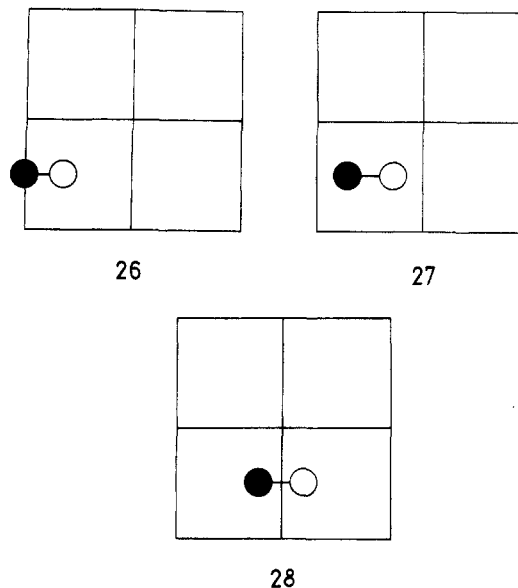| | overlap population | | | $d_{O-Rh}$, | binding |
| geometry | N–O | N–Rh | O–Rh | Å | energy, eV |
|---|---|---|---|---|---|
| 21 | 0.85 | 0.42 | 0.12 | 2.44 | 1.52 |
| 22 | 0.89 | 0.49 | 0.71 | 1.37 | 3.05 |
| 23 | 0.90 | 0.56 | 0.39 | 1.90 | 2.49 |
| 24 | 0.85 | 0.40 | 0.02 | 3.79 | 1.39 |
| 25 | 0.98 | 0.52 | 0.38 | 1.90 | 2.09 |
| 26 | 0.96 | 0.34 | 0.07 | 2.44 | 0.97 |
| 27 | 0.94 | 0.47 | 0.31 | 1.90 | 1.93 |
| 28 | 1.00 | 0.24 | 0.12 | 1.90 | 1.98 |

cussed in the previous section. These include not only the point reached at 90° from on-top or bridging linear origins but other geometries as well.

Some computational results for these geometries are compared in Table VI. Let us discuss them one by one. In **21**, obtained by bending from the linear geometry, we lose the N–surface interaction (the N–Rh overlap population gets smaller) and gain a new oxygen–surface interaction (see Table IV). As we bend NO from a linear to a lying down position, **22**, starting in the bridging position, the nitrogen completely loses its bonding interaction with the rhodium atom toward which the NO bends and the oxygen atoms comes very close to this Rh atom, acquiring a large positive overlap population (see Table V). It seems likely that the NO group as a whole will shift, in response to bonding effects, to a geometry such as **23**. For this geometry, we have set both N–Rh and O–Rh distances equal to 1.90 Å and kept the N–O distance at 1.15 Å, as earlier.

Another bending possibility from an on-top position is toward a fourfold hollow, leading to **24**. The bending is also accompanied by a decrease in N–Rh and N–O overlap populations. This bending is not energetically favored, at least not if the position of the N atom is fixed during the bending. One possible change might be to move the N atom along the diagonal of the (100) face, to reach the geometry shown in **25**. In this case too, the N–Rh and O–Rh distances are 1.90 Å, and the N–O distance is 1.15 Å as before. In going from **24** to **25**, the $2\pi$–surface interaction decreases, but all the other NO orbitals are more involved in bonding, especially the $4\sigma$ and $5\sigma$. As a consequence of this, the N–O overlap population is much larger in **25**, and so are the N–Rh and O–Rh overlap populations. This movement is energetically favored.

Another possible geometry considered for lying down NO originates from bending from the bridging position toward the fourfold hollow **19**. The top view of NO lying down in this geometry is shown in **26**. During this bending, the binding energy increases continuously, the N–O overlap population increases after an initial drop at $\phi$ = 45°, and the N–Rh overlap population constantly decreases. Since by this bending we are gaining some new attrac-

tive O–surface interactions, one again expects further motion to optimize these interactions. The NO group can move "right" from the position shown in **26** to reach a more symmetrical position, shown in **27**, or it can move "left" to occupy a position where it lies perpendicular to the Rh–Rh surface bond, directly above its midpoint, as shown in **28**. In going from **26** to **27**, the interaction of



26                  27



28

the $4\sigma$ and $5\sigma$ orbitals with the surface orbitals increases, the $1\pi$ orbital's electron densities decrease, and the $2\pi$ orbital increases slightly. As a result of these changes, the N–O overlap population decreases somewhat, and overlap populations between oxygen and nitrogen atoms with the surface increase. The N–Rh and O–Rh overlap populations in Table VI refer to the nearest surface Rh atoms. The changes in these overlap populations lead to a higher binding energy, and this movement is energetically favored. The same is true on going from **26** to **28**. But the bonding pattern and consequently the NO $\sigma$ orbitals densities are quite different. The NO $\sigma$ orbitals do not have a suitable geometry for interaction with the surface atom any more. The overall interaction goes primarily through NO $\pi$ orbitals, but the total NO $2\pi$ orbital filling is slightly smaller that in **26** and **27**, so the N–O overlap population is higher. Still, the total energy change is essentially the same as in **27**.

In conclusion, we can say that a geometry for a highly inclined or lying down NO on the Rh(100) surface, according to our calculations, is likely to be **23**, although **25** and **27** should not be disregarded as possible candidates. It should be noted again that **27** was proposed[81] to be the lying down NO geometry. It is very hard to give a definitive answer to this question using our computational method. The discussion in this section was partly based on energetic arguments. In general, we tend to avoid such because of our unwillingness to trust the total energies given by the extended Hückel method.

## Coadsorption of NO and CO

Campbell and White[57] have examined nitric oxide reduction with carbon monoxide on polycrystalline rhodium wire, using flash desorption spectroscopy (FDS). They found that adsorbed NO molecules dissociate into adsorbed nitrogen and oxygen. Oxygen reacts with either adsorbed or gas-phase CO to form carbon dioxide. Dubois et al.[6] have reported evidence for an oxygen intermediate in the NO/CO process on the Rh(331) single-crystal surface using

**Table VII. Coadsorption of CO and NO on the Rh(100) Surface (31) with the NO Bending toward the Fourfold Hollow**

| | $\phi$ | 0° | 45° | 90° | 110° |
|---|---|---|---|---|---|
| CO electron densities | $5\sigma$ | 1.67 | 1.67 | 1.64 | 1.65 |
| | $2\pi_x$ | 0.35 | 0.36 | 0.32 | 0.66[a] |
| | $2\pi_y$ | 0.36 | 0.37 | 0.34 | |
| NO electron densities | $5\sigma$ | 1.72 | 1.75 | 1.75 | 1.79 |
| | $2\pi_{x(z)}$ | 0.85 | 0.99 | 1.04 | 1.98[a] |
| | $2\pi_y$ | 1.27 | 1.29 | 1.06 | |
| overlap populations | C–O | 1.24 | 1.23 | 1.25 | 1.26 |
| | C–Rh(1) | 0.86 | 0.85 | 0.81 | 0.83 |
| | N–O | 0.92 | 0.89 | 0.96 | 1.00 |
| | N–Rh(3) | 0.55 | 0.50 | 0.34 | 0.27 |
| | C–O$_{NO}$ | 0.00 | 0.03 | 0.05 | 0.01 |
| binding energy, eV | | 6.26 | 5.60 | 3.43 | 3.26 |

[a] The total over two $2\pi$ orbitals.

HREELS and AES and indicated that under their reaction conditions the formation of gaseous molecular nitrogen is a fast process. Two mechanistic studies came from the work of G. B. Fisher[58b,58c] and Hendershot and Hansen.[60] The first studied the reaction on the Rh(111) surface and concluded that the rate-determining step (also for CO/O₂ reaction) is CO(a) + O(a) → CO₂ (gas). In recent work,[58e] they argued about the possibility of a true bimolecular reaction being involved on Rh(111) surface, with the rate-limiting step in formation of N₂ by the recombination of adsorbed N atoms and that the reaction rate on Rh(100) is significantly different from the one on Rh(111) surface. The second contribution is more interesting for us since it deals with CO/NO processes on the Rh(100) surface. The authors found that this process is selective toward the production of N₂ and CO₂, but that some other steps must be present in the mechanism, including the formation and decomposition of N₂O and NO₂ adsorbed species. Also, they stated that the NO dissociation, i.e., adsorbed atomic oxygen, does not play an important role in the higher reactant partial pressure conditions. Villarrubia and Ho[61] also reported low coverage adsorption effects of lying down NO with O₂, NO, and CO, and they concluded that coadsorbates will convert the lying down $\alpha_1$ NO into a vertically bonded one, with CO being about 2 times less effective than O₂ and NO. Recently, Peden et al.[59] investigated the kinetics of CO oxidation by NO or O₂ on the Rh(111) and Rh(100) surfaces. They concluded that CO oxidation with NO on the Rh(111) surface fits the proposed mechanism[58e] but that the rate-limiting step on Rh(100) is N₂ formation from adsorbed NO and N species.

Now let us investigate the coadsorption of CO and NO on the Rh(100) surface with our calculational tools. The procedure that we will adopt is to put CO and NO on the surface at the same time in representative positions suggested by experimental studies. By following the trends in orbital electron density and overlap population changes, we can look for indicators of NO bond weakening and CO₂ formation.

There are a large number of possible arrangements of CO and NO on this surface, as both can, in principle, assume bridging or on-top adsorption sites. Let us first consider the situation where CO and NO are 3.80 Å apart (the surface until cell diagonal). Two possibilities are one with both CO and NO being in bridging positions (29) and one with both in on-top positions (30). The overlayer has a c(2×2) structure in both cases comprised of p(2×2) structures of the individual absorbates giving a total coverage of 1/2. The drawings give a perspective view showing only the surface layer of the Rh slab. The

big circles represent Rh atoms, while C, N, and O atoms are indicated. The coordinate system is the same that was shown in 14.



⊕–C
●–N
○–O
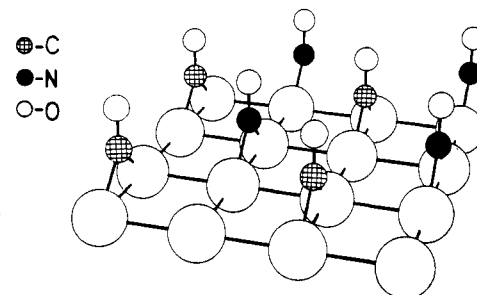
29
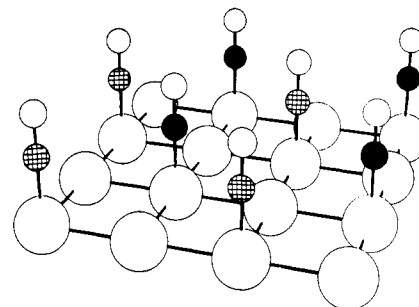


30

In these geometries, CO and NO do not "feel" each other very much. The overlap populations and electron densities have not changed significantly from the case of individual adsorption. This is consistent with our previous conclusion that the coadsorbate interactions for both the CO and NO are not significant for distances greater than the van der Waals radii.

For 29, we considered the bending of NO with the bending angle $\phi$ being defined as before. The bending direction is toward the fourfold hollow, so $C_{CO}$ and $O_{NO}$ would come closer as the bending angle approaches 90°.

With bending, the NO and N–Rh overlap populations do not seem to be affected much by the presence of CO, since they are nearly the same as they were in 19. The C–O overlap population increases, and the C–Rh overlap population decreases relative to the case of CO adsorption. There is a very weak repulsive interaction between the adsorbates, partly due to through-space 1π–1π repulsive interaction. The differences are small compared to 1/2 coverage adsorption of each individual adsorbate. The origin of this so-called "repulsion" may be competition of the CO and NO for surface electron density.

A similar situation is observed when both CO and NO are in on-top positions, 30, with the bending direction of NO being along the surface Rh–Rh bond.

It is clear that, in these geometries with a total coverage of 1/2, CO and NO are too far apart to interact strongly. Therefore, to model the reactivity of CO and NO, these two adsorbates must approach each other in a realistic way. One possibility has the same initial geometry as in 30, but this time the bending is toward the fourfold hollow and, hence, the oxygen of the NO moves closer to the CO molecule. For a bending angle of 90°, the $O_{NO}$–$C_{CO}$ distance becomes 2.65 Å, and the overlap population beteen them is still negligible. We can see some of the coadsorption effects, but they are still weak. The adsorbates may be too far away for a significant through-space interaction, or this geometry may not be suitable for effective orbital interaction. To achieve the

values of the O–C–O angle in the transition-metal complexes of $CO_2$,[88] the NO bending angle was increased to 110°. No significant changes were produced, however.

Several other possibilities exist which will provide for shorter contacts between the $C_{CO}$ and $O_{NO}$. These include increasing the total adsorbate coverage or making adjustments in the adlayer structure. The previous discussion was based on an overall c(2×2) pattern comprised of p(2×2) patterns of each adsorbate.
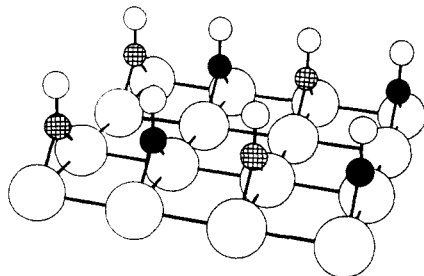
We can imagine such a situation where CO is adsorbed on top and NO in the two-fold bridging position, as shown in **31**. These are the sites that CO and NO would prefer
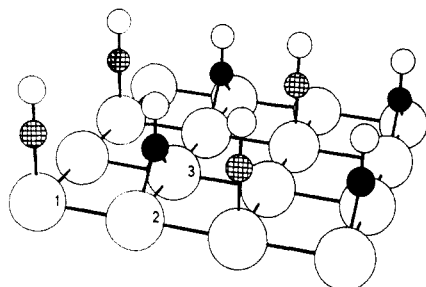


31

in the absence of competing coadsorbate interactions. The results of our calculations for this geometry are summarized in Table VII. The coadsorption effect for $\phi = 0°$ is somewhat stronger now and is reflected in higher C–O and N–O overlap populations. This is consistent with HREELS data showing higher CO and NO stretching frequencies with increasing coverages, i.e., with the presence of repulsive interactions. Some decrease in C–surface and N–surface interaction is expected, but in our calculations, these overlap populations are essentially the same. The N–Rh(3) overlap population is somewhat higher than when NO is adsorbed alone and is suspected to be a consequence of CO–NO repulsion. With further bending, we gain some attractive C–$O_{NO}$ interaction, but the repulsive interactions are stronger, so that the C–surface interaction is reduced and C–O overlap population increased. The energetics of these changes show a constant decrease in binding energies, so that we could conclude that this arrangement does not lead to desired changes, either. These coadsorption efects can support the experimental finding of Villarrubia and Ho[81] that lying down NO will be converted into a vertically bonded one when coadsorbed with CO.

Another possible arrangement of coadsorbed CO and NO is shown in **32**. Both adsorbates are in bridging posi-



32

(88) (a) Alvarez, R.; Cormona, E.; Marin, J. M.; Poveda, M. L.; Gutierrez-Puebla, E.; Monge, A. *J. Am. Chem. Soc.* **1986**, *108*, 2286. (b) Aresta, M.; Nobile, C. F.; Albano, V. G.; Formi, E.; Manassero, M. *J. Chem. Soc., Chem. Commun.* **1976**, 636. (c) Fachinetti, G.; Floriani, C.; Zanazzi, P. F. *J. Am. Chem. Soc.* **1978**, *100*, 7405.

tions, but now the overall adsorption geometry gives a 2×1 structure with nearest-neighbor coadsorbate interactions of 2.69 Å. The NO bending direction is toward the fourfold hollow.

Again, when NO is linear there is no significant coadsorption effect. CO shows the same effects whether the nearest-neighbor adsorbate is NO or another CO. Of course, things change when NO starts to bend since the C–$O_{NO}$ distance is getting smaller. For $\phi = 0°$, the distance between carbon and nitric oxide oxygen is 2.92 Å, and when NO bends to 45°, it is reduced to 2.02 Å. At this distance, we can expect some interaction, and it is reflected in the small positive C–$O_{NO}$ overlap population of 0.02.

The C–O and C–Rh overlap populations are reduced. Also, there is a small repulsive interaction between the carbon and nitrogen (a small negative overlap population of –0.02). When NO is lying down, the carbon and nitric oxide oxygen are now only 1.54 Å apart, and the orientation of the CO $\pi_x$ and NO 5$\sigma$ orbitals is suitable for a strong interaction. This results in a large positive C–$O_{NO}$ overlap population of 0.45, compared to the value for a C–O single bond of 0.56. The occupation of the CO 2$\pi$ orbitals increases, and the bond strength decreases. The C–surface interaction is weaker, since the CO 2$\pi$ orbitals now interact with NO. But, as in the case when NO is lying down alone on the surface, the N–surface interaction is highly reduced, and even additional interaction with CO is not strong enough to weaken the NO bond further. A significant bonding interaction is observed between $C_{CO}$ and $O_{NO}$ though.

Another possibility of CO and NO coadsorption is shown in **33**. Here both CO and NO are in on-top positions on the two nearest surface Rh atoms.
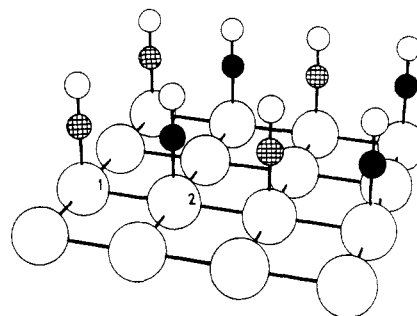


33

The CO–NO distances are the same as in a previously discussed geometry, **32**. Again, the NO bending is in the $xz$ plane, and the calculations were performed for the three bending angles. The results are summarized in Table VIII.

This situation is reasonable, as CO prefers on-top geometries on Rh(100), and on the Rh(111) surface NO shifts from two-fold bridging positions to on-top sites when oxygen is present on the surface.[51] Let us first discuss the coadsorption effects for $\phi = 0°$ and compare the results to those for individual adsorption of CO and NO. There are no changes in 4$\sigma$ and 1$\pi$ orbitals of CO and NO (not shown in the table). In this geometry, the degeneracy of the 2$\pi$ orbitals is removed, and these are considered separately. The CO 2$\pi$ orbitals are less populated than for CO on Rh(100) (see Table I), and consequently, the C–O overlap population is larger. The same is true for NO (see Table III). Both the C–Rh and N–Rh overlap populations are smaller. This represents a weaker interaction with the surface and would result in a greater CO or NO stretching frequency.

Table VIII. Coadsorption of CO and NO on the Rh(100) Surface in the On-Top Positions with NO Bending in the xz Plane (See 33)

| | $\phi$ | 0° | 45° | 90° | 110° |
|---|---|---|---|---|---|
| CO electron densities | $5\sigma$ | 1.66 | 1.67 | 1.64 | 1.61 |
| | $2\pi_x$ | 0.33 | 0.43 | 0.73 | 0.59 |
| | $2\pi_y$ | 0.35 | 0.35 | 0.42 | 0.38 |
| NO electron densities | $5\sigma$ | 1.70 | 1.72 | 1.55 | 1.62 |
| | $2\pi_{x(z)}$ | 0.99 | 1.23 | 0.98 | 1.02 |
| | $2\pi_y$ | 0.97 | 0.98 | 1.25 | 1.48 |
| overlap populations | C–O | 1.24 | 1.20 | 1.02 | 1.12 |
| | C–Rh(1) | 0.86 | 0.87 | 0.69 | 0.68 |
| | N–O | 0.91 | 0.87 | 0.88 | 0.82 |
| | N–Rh(2) | 0.72 | 0.66 | 0.42 | 0.28 |
| | C–N | 0.01 | -0.03 | -0.05 | -0.04 |
| | C–O$_{NO}$ | 0.00 | 0.04 | 0.47 | 0.38 |
| | O$_{NO}$–Rh(1) | 0.00 | 0.05 | -0.03 | 0.00 |
| binding energy, eV | | 5.34 | 3.81 | 2.50 | 1.98 |

The coadsorbate interaction is stronger when NO bends to 45°. The C–O overlap population is significantly reduced due to the $C_{CO}$–$O_{NO}$ interaction, which now has a positive overlap population of 0.04. The N–Rh and C–Rh overlap populations are reduced, but the N–O overlap population is greater than in the case of single NO adsorption. Evidently, these changes are a consequence of overall repulsive interactions.

With further bending of NO to 90°, the C–O and C–Rh overlap populations are reduced further. The N–O overlap population is somewhat larger and, in fact, greater than when the NO is adsorbed alone in the same geometry (0.88 vs 0.85). We have significant interaction between carbon and nitric oxide oxygen with an overlap population of 0.47. The $C_{CO}$–$O_{NO}$ distance is the same as in 32, but here they interact more.

For $\phi$ = 0°–90°, the trend in binding energy is toward weaker adsorption, but with further bending to 110°, the overall interaction becomes more attractive, with binding energy rising again. The C–O overlap population is somewhat larger, but the C–Rh interaction is reduced further. The N–O overlap population is smaller (0.82) than when the NO is alone at the surface in the same position (0.84).

In general, with this bending, we are approaching the situation where there is a tendency for $CO_2$ formation, but the energetic changes in these systems are not favorable. We even tried to calculate this system with smaller initial bending angles of 15° and 30° to investigate the energy changes, but the energy differences of these systems (5.23 and 4.85 eV, respectively) indicate a constant decrease in binding energies with bending.

We can also imagine coadsorption geometries where both the CO and NO are in the bridging positions, being bound to the same surface Rh atom. One of two such possibilities is shown in 34, where CO and NO are bridging mutually perpendicular surface Rh–Rh bonds. Here
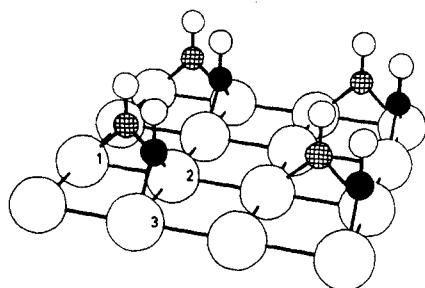


34

we can imagine two possible ways of NO bending in the xz plane and the bending toward the "common" surface atom, i.e., bending in the yz plane. The results are shown in Table IX. The coadsorption effect is the strongest here, since the adsorbates are very close to each other. The carbon and nitrogen are only 1.90 Å apart. As in the case of high coverage, both C–O and N–O have larger overlap populations than when they are alone at the surface. The C–surface and N–surface interactions are weakened, with respect to the common Rh(2) atom, while for the other Rh atoms the overlap populations are slightly larger compared with the single adsorbate studies. Also, there is a certain C–N attractive interaction which occurs primarily through their $\pi$ orbitals, including $1\pi$ orbitals. The carbon and nitric oxide oxygen do not interact, since they are, in this geometry, still quite far away from each other (2.28 Å).

Let us now discuss the NO bending in the xz plane. For $\phi$ = 45°, the C–O and N–O overlap populations are further reduced. While the overall C–surface interaction remains essentially the same, the N–surface interaction is reduced. The weakening of the C–O bond is mainly due to the oxygen–oxygen interaction, which presumably goes through the $1\pi$ orbitals (not shown in Table IX); some go through the NO $\sigma$ orbitals. We still have some positive C–N overlap populations and a small positive carbon–oxygen (from NO) overlap population of 0.05, as the C–O$_{NO}$ distance is now 1.66 Å. When we bend the NO further, $\phi$ = 90°, this distance is reduced to 1.36 Å, which results in a high C–O$_{NO}$ interaction with an overlap population of 0.54. The C–O overlap population is reduced to 0.91. The N–O overlap population (0.93) is now larger than for $\phi$ = 45°, due to the smaller N–surface interaction, but smaller with respect to NO alone at the surface in the same geometry. This geometry is showing a strong tendency for $CO_2$ formation and some small effect to reduce the N–O bond strength, but the energetics of these changes do not really favor them.

The bending of NO to 45° in the yz plane, toward the surface Rh(2) atom, is energetically unfavorable. The trends in overlap population are very similar to those of bending in the xz plane, except for the N–surface overlap populations. They change logically, and the N–Rh(2) overlap population decreases significantly. N–Rh(3) decreases also, though not as much. Both are much smaller than the corresponding values when NO is alone at the surface. When NO is lying down in this arrangement, the carbon and oxygen from NO are again very close to each other (1.36 Å), only now the Rh(2) surface atom is "between" them. Again $4\sigma$ and $1\pi$ CO and NO orbitals are strongly involved in bonding. There is a depopulation of the NO $1\pi$ orbitals and greater donation into the $2\pi$ orbitals. Hence, the N–O overlap population is reduced. The C–O overlap population is larger than when $\phi$ = 45°, but still much lower than when CO is alone at the surface. The N–Rh(2) overlap population is negative, and the overlap population between carbon and $O_{NO}$ strongly increases. The CO–surface interaction is further reduced, with a C–Rh(2) overlap population of only 0.13, so that the CO is weakly bound to the surface now. If we have a situation in which weakly bound NO species (lying down or highly inclined) at the surface approached coadsorbed COs, in this geometry, then $CO_2$ and N species are possible products, with $CO_2$ being weakly bound to the surface.

Finally, we suggest a possible geometry where both CO and NO are in a bridging position and bound to adjacent Rh atoms as shown in 35. The bending of NO is in the

**Table IX. Coadsorption of CO and NO on the Rh(100) Surface (See 34) with NO Bending in *xz* and *yz* Planes**

| | $\phi$ | 0° | xz plane | | yz plane | |
|---|---|---|---|---|---|---|
| | | | 45° | 90° | 45° | 90° |
| CO electron densities | $5\sigma$ | 1.67 | 1.67 | 1.67 | 1.67 | 1.65 |
| | $2\pi_x$ | 0.72 | 0.72 | 0.64 | 0.61 | 0.84 |
| | $2\pi_y$ | 0.46 | 0.41 | 0.86 | 0.46 | 0.42 |
| NO electron densities | $5\sigma$ | 1.71 | 1.60 | 1.76 | 1.61 | 1.62 |
| | $2\pi_{x(z)}$ | 0.87 | 1.05 | 1.01 | 1.00 | 1.08 |
| | $2\pi_{y(z)}$ | 1.22 | 0.98 | 1.10 | 0.96 | 1.21 |
| overlap populations | C–O | 1.11 | 0.96 | 0.91 | 0.99 | 1.02 |
| | C–Rh(2) | 0.47 | 0.47 | 0.36 | 0.38 | 0.14 |
| | C–Rh(1) | 0.63 | 0.64 | 0.50 | 0.64 | 0.65 |
| | N–O | 0.95 | 0.91 | 0.93 | 0.93 | 0.84 |
| | N–Rh(2) | 0.41 | 0.40 | 0.33 | 0.22 | −0.04 |
| | N–Rh(3) | 0.55 | 0.47 | 0.35 | 0.48 | 0.49 |
| | C–N | 0.16 | 0.04 | −0.05 | 0.07 | 0.01 |
| | C–O$_{NO}$ | −0.08 | 0.05 | 0.54 | 0.04 | 0.46 |
| | O–O | −0.04 | 0.28 | −0.11 | 0.25 | −0.10 |
| | O$_{NO}$–Rh(2) | −0.07 | | | −0.10 | 0.47 |
| binding energy, eV | | 4.72 | 0.79 | 0.86 | −0.30 | 1.59 |

**Table X. CO and NO Coadsorbed on the Rh(100) Surface in the Geometry Shown in 35 with NO Bending in the *xz* Plane**

| | $\phi$ | 0° | 45° | 90° |
|---|---|---|---|---|
| CO electron densities | $5\sigma$ | 1.68 | 1.66 | 1.65 |
| | $2\pi_x$ | 0.77 | 0.74 | 0.70 |
| | $2\pi_y$ | 0.44 | 0.45 | 0.42 |
| NO electron densities | $5\sigma$ | 1.72 | 1.72 | 1.44 |
| | $2\pi_{x(z)}$ | 1.23 | 0.73 | 1.32 |
| | $2\pi_y$ | 0.81 | 0.93 | 0.96 |
| overlap populations | C–O | 1.10 | 1.10 | 1.08 |
| | C–Rh(2) | 0.62 | 0.54 | 0.26 |
| | C–Rh(1) | 0.62 | 0.61 | 0.62 |
| | N–O | 0.94 | 1.06 | 0.85 |
| | N–Rh(2) | 0.54 | 0.31 | −0.02 |
| | N–Rh(3) | 0.54 | 0.53 | 0.45 |
| | C–N | 0.01 | −0.02 | −0.03 |
| | C–O$_{NO}$ | 0.00 | 0.02 | 0.33 |
| | O–O | 0.00 | −0.08 | −0.10 |
| | O$_{NO}$–Rh(2) | −0.08 | −0.09 | 0.56 |
| binding energy, eV | | 4.98 | 5.53 | 4.82 |

*xz* plane here, toward the Rh(2) atom. The results are given in Table X.
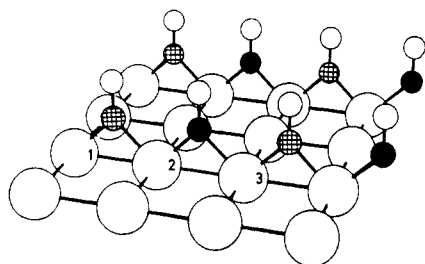


**35**

The coadsorption effect is not strong (for $\phi = 0°$) but is notable. The occupation of the CO $2\pi$ orbitals is larger than when CO is alone at the surface (see Table I), but the CO overlap population is somewhat larger. This is due to a weaker CO–surface interaction. The same is true for NO (see Table III). Again, this is consistent with the experiments which suggest that, at high coverages, the stretching frequencies shift to larger values and the desorption temperatures decrease.

For the bending angle of 45°, both CO– and NO–surface interactions are reduced. This effect is greater for NO and is reflected in a lower occupation of the $2\pi$ orbitals and larger N–O overlap population. We cannot see significant interaction of the oxygen from NO with the

carbon and Rh(2) atoms, even though the distances of 2.04 and 2.22 Å, respectively, suggest that some interaction might occur. When NO is lying down, these distances are reduced to 1.54 and 1.36 Å, respectively. The CO–surface interaction is reduced, and the nitrogen loses its interaction with the surface Rh(2) atoms. The N–surface interaction here is smaller than in the case of individual NO adsorption. The N–O overlap population is strongly reduced and is smaller than when NO is alone at the surface in the same geometry (0.89, Table V). As it was proposed earlier, this may be a candidate for the NO dissociation mechanism. The C–O overlap population is also further reduced. The oxygen–oxygen overlap population is negative, and oxygen from NO is now more weakly bound to the Rh(2) atom than in the case of individual NO adsorption (0.71, Table V). CO can interact with the lying down NO species at the surface in this geometry, the trends for $CO_2$ formation and N–O bond breaking are evident.

To conclude this section, we point out that most of the NO bending mechanisms do not favor the CO/NO reaction but that there are several arrangements, with NO lying down at the surface, which would lead to N–O bond breaking and $CO_2$ formation. So, perhaps, we do not need the NO dissociation as a necessary precondition for this reaction to occur. In that sense, we could support the conclusion of Hendershot and Hansen[60] that the NO dissociation is not important under their reaction conditions. On the other hand, we find the strongest efects if NO is lying down along the bridged surface Rh–Rh bond (as in 34 and 35), i.e., the only possible candidate for a NO dissociation mechanism in the frame of our bending scheme. But, we were able to produce the desired trends, though to a smaller extent, in some other geometries, as in 34 when NO is lying down with the oxygen being close to a fourfold hollow site (as in 26) or even in 33, with the bending angle greater than 90°.

### Coadsorption of CO and Oxygen

Up to now, in all the coadsorption geometries, we applied the bending model for NO dissociation. We have found several geometries of lying down NO with which the CO could readily react to form $CO_2$. Now we would like to briefly investigate the coadsorption of CO and oxygen, as the interaction of such species is suggested to be the rate-determining step for the CO/NO reaction on Rh(111). The reaction of CO and O (or $O_2$) on various transition metals has been widely investigated,[89] as well as their reaction on various Rh surfaces.[58d,59,90] The adsorption

of oxygen on Rh surfaces has been investigated experimentally.[3,66,82,91] On the Rh(100) surface,[82] oxygen is dissociatively adsorbed in three $\beta$ states, and there is a low-temperature molecular adsorption state. Here we assumed that the $O_2$ has dissociated and that the oxygen atoms are found in fourfold hollow sites.[66] The Rh–O distance of 2.05 Å was taken from the corundum structure of a $Rh_2O_3$ system.[92]

Keeping the oxygen in the fourfold hollow, we have two possible ways to obtain a close C–O(ads) contact. The first is on-top sites as in 36, and the second is with CO in the twofold bridging position, 37. The C–O(ads) distances are 2.29 and 1.53 Å, respectively. The results for these sites are presented in Table XI.
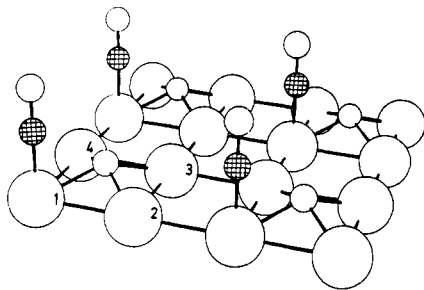


36
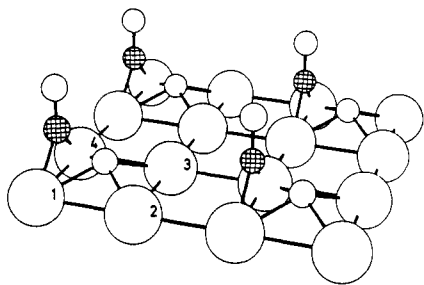


37

Let us discuss the geometry where the CO is on top, 36. When coadsorbed with the oxygen, the degeneracy of CO $\pi$ orbitals is removed, but the differences between these orbitals are small. Also, the oxygen $p_x$ and $p_y$ orbitals lose their degeneracy, and that effect is slightly greater. CO $2\pi$ and $5\sigma$ orbitals are somewhat depopulated when compared with CO being alone at the surface. The same is true for oxygen $p_x$ and $p_y$ atomic orbitals. The C–O overlap population increases. This geometry does not provide for efficient C–O(ads) interaction, as the C–O distance is prohibitively long. Instead, we see repulsive interaction of coadsorbates and weaker adsorbate surface bonding.

In the case where CO is in the bridging position, the coadsorbates are closer to each other, and CO $\pi$ and oxygen p orbitals are collinear, so it is logical to expect more interaction. Indeed, the changes in electron densities and

Table XI. Coadsorption of CO and O on the Rh(100) Surface in the Geometries Shown in 36 and 37

| | | 36 | CO or O alone[a] | 37 | CO or O alone[a] |
|---|---|---|---|---|---|
| CO electron densities | $4\sigma$ | 1.78 | 1.78 | 1.61 | 1.72 |
| | $1\pi_x$ | 1.99 | 1.99 | 1.90 | 1.90 |
| | $1\pi_y$ | 1.99 | 1.99 | 1.95 | 1.95 |
| | $5\sigma$ | 1.64 | 1.67 | 1.58 | 1.69 |
| | $2\pi_x$ | 0.32 | 0.36 | 0.61 | 0.47 |
| | $2\pi_y$ | 0.32 | 0.36 | 0.73 | 0.74 |
| O electron densities | d | 1.79 | 1.78 | 1.72 | 1.78 |
| | $p_x$ | 1.46 | 1.49 | 1.30 | 1.49 |
| | $p_y$ | 1.48 | 1.49 | 1.45 | 1.49 |
| | $p_z$ | 1.92 | 1.92 | 1.75 | 1.92 |
| overlap populations | C–O | 1.26 | 1.23 | 1.04 | 1.10 |
| | C–Rh(1) | 0.82 | 0.86 | 0.44 | 0.62 |
| | $O_a$–Rh(1) | 0.20 | 0.23 | 0.12 | 0.23 |
| | $O_a$–Rh(2) | 0.23 | 0.23 | 0.24 | 0.23 |
| | C–$O_a$ | 0.01 | | 0.47 | |

[a] CO in on-top or bridging sites, singly adsorbed in a p(2×2) structure; O in fourfold hollow site, singly adsorbed in a p(2×2) structure.

Table XII. Extended Hückel Parameters

| orbital | $H_{ii}$, eV | $\zeta_1$ | $\zeta_2$ | $C_1$[a] | $C_2$[a] |
|---|---|---|---|---|---|
| Rh 5s | −7.31 | 2.13 | | | |
| Rh 5p | −3.39 | 2.10 | | | |
| Rh 4d | −10.35 | 4.29 | 1.97 | 0.5807 | 0.5685 |
| C 2s | −18.20 | 1.63 | | | |
| C 2p | −9.50 | 1.63 | | | |
| N 2s | −23.95 | 1.95 | | | |
| N 2p | −10.95 | 1.95 | | | |
| O 2s | −27.61 | 2.28 | | | |
| O 2p | −11.01 | 2.28 | | | |

[a] Contraction parameters used in the double-$\zeta$ expansion.

overlap populations are much greater than in the previous case. The C–O overlap population is reduced, and we gain a positive C–O(ads) overlap population of 0.46. At the same time, the C–Rh(1) overlap population is reduced as are the overlap populations between the adsorbed oxygen and surface rhodium. The geometry looks promising for the formation of $CO_2$ molecules at the surface and subsequent desorption as well.

## Appendix

In this paper, all performed computations are tight-binding band calculations of the extended Hückel type. The $H_{ii}$ values for rhodium were obtained by charge iteration on the bulk metal (with the experimental fcc geometry) using Gray's equation[93] with A, B, and C parameters taken from ref 94. The carbon $H_{ii}$ values were taken from an earlier work of this group[16] and were in good agreement with iterated values. The oxygen $H_{ii}$ values were obtained by charge iteration on CO adsorbed on both sides of the rhodium three-layer slab, keeping the C and Rh $H_{ii}$ values constant, with low coverage of 0.25 on both sides to avoid the adsorbate interactions. Nitrogen $H_{ii}$ values were obtained for NO adsorbed in the same way as CO, with the same procedure, with oxygen and rhodium parameters being constant. Oxygen parameters were previously determined parameters from CO

(89) (a) Odörfer, G.; Plummer, E. W.; Freund, H.-J.; Kuhlenbeck, H.; Neumann, M. *Surf. Sci.* **1988**, *198*, 331. (b) Shinn, N. D. *Langmuir* **1988**, *4*, 289. (c) Berlovitz, P. J.; Peden, C. F. H.; Goodman, D. W. *J. Chem. Phys.* **1988**, *92*, 5213. (d) Szabò, A.; Kiskinova, M.; Yates, J. T., Jr. *J. Chem. Phys.* **1989**, *90*, 4604.

(90) (a) Gurney, B. A.; Ho, W. *J. Chem. Phys.* **1987**, *87*, 1376. (b) Goodman, D. W.; Peden, C. F. H. *J. Phys. Chem.* **1986**, *90*, 4839. (c) Schwartz, S. B.; Schmidt, L. D.; Fischer, G. B. *Ibid.* **1986**, *90*, 6194. (d) Brown, L. S.; Sibner, S. J. *J. Chem. Phys.* **1988**, *89*, 1163. (e) Li, Y.-E.; Gonzalez, R. D. *J. Phys. Chem.* **1988**, *92*, 1589. (f) Panayotov, D.; Basu, P.; Yates, J. T., Jr., *Ibid.* **1988**, *92*, 6066.

(91) (a) Castner, D. G.; Somorjai, G. A. *Surf. Sci.* **1979**, *83*, 60. (b) Thiel, P. A.; Yates, Y. T.; Weinberg, W. H. *Surf. Sci.* **1979**, *82*, 22. (c) Campbell, C. T.; White, J. M. *J. Catal.* **1978**, *54*, 289.

(92) Coey, J. B. M. *Acta Crystallogr.* **1970**, *B26*, 1876.

(93) Ballhausen, C. J.; Gray, H. B. *Molecular Orbital Theory*; W. A. Benjamin: New York, **1965**; p 125.

(94) Munita, R.; Letelier, J. R. *Theor. Chim. Acta* **1981**, *58*, 167.

adsorption. *B* and *C* iteration parameters for C, N, and O atoms were taken from ref 95. Extended Hückel parameters for all atoms used are listed in Table XII.

(95) McGlyn, S. P.; Vanquickenborne, L. G.; Kinoshita, M.; Carroll, D. G. *Introduction to Applied Quantum Chemistry*; Holt, Rinehart and Winston: New York, 1964; pp 423–431.

All the results listed in this paper are from the single-face adsorption calculations, using the three-layer slab model. The geometrical parameters for coadsorption are as follows: C–O, 1.15; N–O, 1.15; Rh–Rh, 2.6893; Rh–C, 1.90; Rh–N, 1.90; and Rh–O, 2.05 (all values in Å). The *k*-point sets varied from 49 to 12 points in order to keep the total number of states for each geometry similar.

# Determination of the Electrostatic Potential of Positively Charged Monolayers at the Air/Water Interface by Means of Fluorometric Titration of 4-Heptadecyl-7-hydroxycoumarin

Jordan G. Petrov*

*Department of Physical Chemistry, University of Sofia, 1, Anton Ivanov Ave., 1126 Sofia, Bulgaria*

Dietmar Möbius

*Max-Planck-Institut für biophysikalische Chemie, Postfach 2841, D-3400 Göttingen, FRG*

The electrostatic potentials $\psi_0$ of insoluble monolayer mixtures of a neutral and a positively charged component spread onto an aqueous solution of 0.1 M NaCl are determined by means of fluorometric titration of embedded 4-heptadecyl-7-hydroxycoumarin. Methyl arachidate and dimethyldioctadecyl-ammonium bromide are used, and the surface charge density $\sigma_0$ is varied through their molar ratio. The $\psi_0/\sigma_0$ dependence thus obtained is compared to experimental results reported in the literature for other systems as well as to the Gouy–Chapman theoretical relationship.

## Introduction

The experimental determination of the electrostatic potential $\psi_0$ between a nonconducting phase and an aqueous electrolyte solution is a complicated problem. At the same time, its successful solution is of substantial interest due to the important role this parameter plays in the colloid stability, wetting, biomembrane functioning, cell adhesion, etc.

The development of the theory of thin liquid film stability has enabled the determination of $\psi_0$ from measurements of equilibrium film thicknesses.[1] In this way, $\psi_0$ values for the air/water interface have been obtained by investigation of foam films stabilized with anionic and cationic surfactants.[1-4] However, due to restriction of the theoretical calculation of the electrostatic disjoining pressure, reliable data on $\psi_0$ can be obtained so far at low ionic strengths only.

In the studies of the electrostatic properties of biomembranes and micelles, $\psi_0$ is determined by means of various spectroscopic techniques. Those based on molecular spin probes[5] and interfacial pH indicators[6] are most often employed. In the latter case, $\psi_0$ is evaluated from the difference in the p*K* values of the indicator at the interface and in the bulk, both being determined by following the absorption or fluorescence changes with pH. (In later studies, $\psi_0$ is related to the difference between p$K_i$ in a neutral and a charged interface.[8])

Fromherz et al.,[7-10] as well as some Australian colleagues,[11-14] have contributed substantially to the progress and recent intensive application of this method. These studies deal with neutral and charged micelles and insoluble monolayers transferred onto a hydrophobic solid substrate by means of the Langmuir–Blodgett technique.

In the present investigation, the electrostatic poten-

* To whom correspondance should be addressed.
(1) Derjaguin, B. V.; Titijevskaya, A. *Kolloidn. Zh.* 1953, *15*, 416.
(2) Scheludko, A.; Exerowa, D. *Kolloid-Z.* 1959, *165*, 148; 1960, *168*, 24.
(3) Exerowa, D. *Kolloid-Z.* 1969, *232*, 703.
(4) Exerowa, D. Dr. Sci. Thesis, Bulg. Acad. Sci., Sofia, 1987.

(5) Castle, J. D.; Hubbell, W. L. *Biochemistry* 1976, *15*, 4818.
(6) Haynes, D. H. *J. Membr. Biol.* 1974, *17*, 341.
(7) Fromherz, P. *Biochim. Biophys. Acta* 1973, *323*, 326.
(8) Fromherz, P.; Masters, B. *Biochim. Biophys. Acta* 1974, *356*, 270.
(9) Fernandez, M. S.; Fromherz, P. *J. Phys. Chem.* 1977, *81*, 1755.
(10) Fromherz, P.; Kotulla, R. *Ber. Bunsen-Ges. Phys. Chem.* 1984, *88*, 1106.
(11) Lovelock, B.; Grieser, F.; Healy, T. W. *J. Phys. Chem.* 1985, *89*, 501.
(12) Lovelock, B.; Grieser, F.; Healy, T. W. *Langmuir* 1986, *2*, 443.
(13) Drummond, C. J.; Warr, G. G.; Grieser, F.; Ninham, B. W.; Evans, D. F. *J. Phys. Chem.* 1985, *89*, 2103.
(14) Drummond, C. J.; Grieser, F. *Photochem. Photobiol.* 1987, *45*, 19.